

---

# GEOMETRIC LOCAL PARAMETERIZATION FOR SOLVING HELE-SHAW PROBLEMS WITH SURFACE TENSION

---

A PREPRINT

**Zengyan Zhang and Wenrui Hao**

Department of Mathematics

The Pennsylvania State University, University Park, PA 16802, USA

[zzz5527@psu.edu](mailto:zzz5527@psu.edu) and [wxh64@psu.edu](mailto:wxh64@psu.edu)

**John Harlim**

Department of Mathematics, Department of Meteorology and Atmospheric Science,

Institute for Computational and Data Sciences

The Pennsylvania State University, University Park, PA 16802, USA

[jharlim@psu.edu](mailto:jharlim@psu.edu)

October 17, 2025

## ABSTRACT

In this work, we introduce a novel computational framework for solving the two-dimensional Hele-Shaw free boundary problem with surface tension. The moving boundary is represented by point clouds, eliminating the need for a global parameterization. Our approach leverages Generalized Moving Least Squares (GMLS) to construct local geometric charts, enabling high-order approximations of geometric quantities such as curvature directly from the point cloud data. This local parameterization is systematically employed to discretize the governing boundary integral equation, including an analytical formula of the singular integrals. We provide a rigorous convergence analysis for the proposed spatial discretization, establishing consistency and stability under certain conditions. The resulting error bound is derived in terms of the size of the uniformly sampled point cloud data on the moving boundary, the smoothness of the boundary, and the order of the numerical quadrature rule. Numerical experiments confirm the theoretical findings, demonstrating high-order spatial convergence and the expected temporal convergence rates. The method's effectiveness is further illustrated through simulations of complex initial shapes, which correctly evolve towards circular equilibrium states under the influence of surface tension.

## 1 Introduction

Many natural phenomena in biology, physics, and materials science are governed by systems of partial differential equations (PDEs) with free (moving) boundaries [7, 8, 13, 14, 17], including plaque growth in cardiovascular disease [8, 14], tumor growth in cancer [5, 17, 31], solidification and melting in materials science [1, 12], and moving fluid interfaces in physics [34, 36]. Among these, the Hele-Shaw problem with surface tension stands out as a widely studied model due to its broad applications across both physical and biological systems [7, 9]. Since the pioneering experiments of Hele-Shaw, who confined a fluid between two closely spaced plates [21], and the seminal work of Saffman and Taylor in 1958 [35], this problem has attracted extensive theoretical and experimental attention.

From a mathematical perspective, the Hele-Shaw problem can be studied both analytically and numerically, with an emphasis on understanding solution structures and their dynamics [2, 6]. Over the past few decades, extensions of the Hele-Shaw model incorporating surface tension have arisen from physical and biological applications [4, 7], motivating the development of theoretical frameworks and nonlinear simulation techniques to investigate steady-state solutions. While PDE theory provides valuable insights in certain special cases, in-depth studies often rely on large-scale numerical simulations to compute steady states, trace bifurcations, and analyze stability [16, 17, 15].

For example, bootstrapping methods combined with multi-grid and domain decomposition techniques, along with homotopy approaches, have been used to compute multiple steady-state solutions of the generalized Hele-Shaw problem [16, 17, 18]. Moreover, adaptive homotopy tracking methods enable the detection of bifurcation points and exploration of global solution structures guided by PDE theory [15, 17, 19]. These methods have also been successfully applied to complex biological systems, such as tumor growth models and the evaluation of cardiovascular disease risk [13, 14].

Despite these advances, developing efficient numerical algorithms for complex PDE systems with free boundaries remains a central challenge. For example, rigorous convergence and error analyses have been established for boundary integral methods applied to simplified Hele-Shaw problems without accounting for surface tension [30]. Specifically, the scheme attains first-order accuracy in time ( $L^\infty$  norm) and  $\delta\theta^\rho$  ( $\rho < 1$ ) in space, relying on a global parameterization in the  $\theta$  direction, which limits its ability to handle complex geometries. Furthermore, singular integration in the boundary integral is not addressed in their analysis.

In this paper, we introduce an efficient numerical method for approximating the solution to Hele-Shaw problems with surface tension on complex geometry, with theoretical guarantees. While the formulation can be extended to arbitrary dimensions, we focus on two-dimensional problems with a one-dimensional smooth complex boundary. By “complex boundary”, we refer mathematically to manifolds that cannot be globally parameterized, i.e., whose atlas has more than one chart. Since the boundary is unknown, that is, it is represented only by a finite number of point cloud data lying on a smooth manifold (or boundary curve), we locally parameterize this manifold with Generalized Moving Least Squares (GMLS), a method with solid theoretical foundations [33]. Numerically, this local parameterization effectively represents functions on complex geometries [11, 24, 29]. Our main technical contribution is the systematic application of this local parameterization to discretize the singular boundary integral equation while respecting the underlying manifold. We further support the method with a theoretical study demonstrating the convergence of the scheme in the limit of a large number of uniformly sampled point cloud data.

The remainder of this paper is organized as follows. In Section 2, we give a brief overview of the Hele-Shaw problem with surface tension and its boundary integral formulation. Section 3 presents an overview of the Generalized Moving Least Squares (GMLS) for approximating boundary curvature, the proposed numerical formulation for solving the free boundary problem, and the corresponding theoretical analysis. In Section 4, we rigorously analyze the convergence and error of the proposed discretization. In Section 5, we demonstrate the effectiveness of the proposed method on several test problems, ranging from simple to complex initial boundaries. We conclude the paper with a summary and discussion in Section 6. An Appendix is included to provide the detailed proof of Proposition 4.3.

## 2 Overview of the Hele-Shaw problem with surface tension and its boundary integral formulation

Consider a tissue or material that behaves as a porous medium. The velocity field  $\mathbf{V}$  is described by Darcy's law,  $\mathbf{V} = -\frac{\sigma}{\mu} \nabla p$ , where  $p$  denotes the pressure,  $\sigma$  is the permeability of the medium, and  $\mu$  is the dynamic viscosity of the fluid. Combining with the conservation of mass,  $\nabla \cdot \mathbf{V} = f$ , where  $f : \Omega(t) \rightarrow \mathbb{R}$  represents distributed sources or sinks, leads to the following PDE system with a free boundary,

$$\begin{cases} -\frac{\sigma}{\mu} \Delta p = f & \text{in } \Omega(t), \\ p = \tau \kappa & \text{on } \Gamma(t), \\ \frac{\sigma}{\mu} \frac{\partial p}{\partial \mathbf{n}} = -V_n & \text{on } \Gamma(t). \end{cases} \quad (1)$$

Here,  $\Omega(t)$  denotes the fluid-filled region, and  $\Gamma(t)$  denotes its moving boundary. In this paper, we consider a bounded two-dimensional domain  $\Omega(t) \subset \mathbb{R}^2$  with a closed curve boundary  $\Gamma(t)$  at any fixed time  $t \geq 0$ . In (1),  $\kappa$  denotes the mean curvature (for instance,  $\kappa = R(t)^{-1}$  if  $\Omega(t)$  is a disk of radius  $R(t)$ ). The boundary condition  $p = \tau \kappa$  models the effect of surface tension: the pressure jump across the interface is proportional to the local curvature, which acts to stabilize and regularize the evolving boundary. In classical Hele-Shaw problems without surface tension, the pressure on the boundary is typically prescribed as a constant or a given potential function [22, 28]. The inclusion of surface tension distinguishes the present model, as the boundary pressure is not known a priori but instead couples dynamically to the evolving geometry through curvature. This feature introduces additional analytical and numerical challenges and is a central focus of this work. For simplicity, we normalize parameters and set  $\sigma = \mu$  and  $\tau = 1$  throughout the remainder of the paper. We assume the kinematic boundary condition on the free boundary  $\Gamma(t)$ , which states that the boundary moves in accordance with the velocity  $\mathbf{V}$ , such that its component in the direction of the outward normal  $\mathbf{n}$  is given by

$$V_n = \mathbf{V} \cdot \mathbf{n} = -\frac{\partial p}{\partial \mathbf{n}} \quad \text{on } \Gamma(t),$$

with  $\mathbf{n}$  pointing out of  $\Omega(t)$ .

In this paper, we consider the case  $f = 0$ , which corresponds to the classical Hele-Shaw free boundary problem. This allows us to integrate the governing equations on the free boundary. Denote  $G(\mathbf{x}, \mathbf{y})$  as the Green's function for the Laplacian operator,  $-\Delta$ . Specifically,  $G(\mathbf{x}, \mathbf{y}) = -\frac{1}{2\pi} \ln \|\mathbf{x} - \mathbf{y}\|$  for two-dimensional cases. Then from the Green's third identity [10, 26], we have

$$-\int_{\Omega} G(\mathbf{x}, \mathbf{y}) \Delta p(\mathbf{y}) dV_{\mathbf{y}} - p(\mathbf{x}) = -\int_{\Gamma} \left( G(\mathbf{x}, \mathbf{y}) \frac{\partial p(\mathbf{y})}{\partial \mathbf{n}(\mathbf{y})} - p(\mathbf{y}) \frac{\partial G(\mathbf{x}, \mathbf{y})}{\partial \mathbf{n}(\mathbf{y})} \right) dS_{\mathbf{y}}, \quad \forall \mathbf{x} \in \Omega(t)$$

Setting  $\Delta p = 0$ , incorporating the jump condition and the boundary condition, we arrive at

$$\frac{\kappa(\mathbf{x})}{2} = \int_{\Gamma} \left( -G(\mathbf{x}, \mathbf{y}) V_n(\mathbf{y}) - \kappa(\mathbf{y}) \frac{\partial G(\mathbf{x}, \mathbf{y})}{\partial \mathbf{n}(\mathbf{y})} \right) dS_{\mathbf{y}}, \quad \mathbf{x}, \mathbf{y} \in \Gamma(t),$$

where  $\mathbf{n} = \frac{\nabla \Gamma}{|\nabla \Gamma|}$  with  $\mathbf{n}(\mathbf{y})$  referring to the unit outer normal vector at  $\mathbf{y} \in \Gamma(t)$ , and  $\kappa = \nabla \cdot \mathbf{n}$ .

Therefore, we have reformulated the classical Hele-Shaw free boundary problem (1) with  $f = 0$  as the following system,

$$\left\{ \int_{\Gamma} G(\mathbf{x}, \mathbf{y}) V_n(\mathbf{y}) dS_{\mathbf{y}} = -\frac{\kappa(\mathbf{x})}{2} - \int_{\Gamma} \kappa(\mathbf{y}) \frac{\partial G(\mathbf{x}, \mathbf{y})}{\partial \mathbf{n}(\mathbf{y})} dS_{\mathbf{y}}, \quad \mathbf{x}, \mathbf{y} \in \Gamma(t), \right. \quad (2a)$$

$$\left. \frac{d\mathbf{x}}{dt} = V_n(\mathbf{x}) \mathbf{n}(\mathbf{x}), \quad \mathbf{x} \in \Gamma(t), \right. \quad (2b)$$

where the solution to the boundary integral equation (BIE) (2a) gives the unknown normal velocity  $V_n$  on  $\Gamma(t)$ , which is represented by point clouds without parameterization information, and the kinematic condition (2b) enables the free boundary to evolve forward in time.

### 3 Numerical approximation for the free boundary problems

In this section, we introduce our approach for approximating the solution to (2) through a local representation of the manifold, which naturally allows one to approximate the integration on the boundary directly. We begin with a brief overview of the Generalized Moving Least Squares (GMLS) method, which constructs local manifold charts and approximates higher-order geometric quantities, such as the curvature  $\kappa$  along moving boundaries. Next, we present the quadrature rules used to discretize the boundary integral equation (2a) in space, yielding a corresponding system of algebraic equations. Solving this system in conjunction with a time discretization to (2b) enables us to track the evolution of the boundary  $\Gamma(t)$  over time.

#### 3.1 Generalized Moving Least Squares approximation of the curvature

Given a set of point cloud data  $X = \{\mathbf{x}_i\}_{i=1}^N \subset \mathbb{R}^n$  sampled from a manifold  $\Gamma$  of dimension  $d$ , we denote the set of  $k$ -nearest neighbors for any point  $\mathbf{x}_i$  in  $X$  by  $K(i) = \{\mathbf{x}_{i_1}, \dots, \mathbf{x}_{i_k}\}$ . In this notation,  $\mathbf{x}_i = \mathbf{x}_{i_1}$ . We can obtain a local estimation of the tangent space at each point by the classical local SVD method stated as follows,

1. Construct the distance matrix  $\mathbf{D}_i := [\mathbf{D}_{i_1}, \dots, \mathbf{D}_{i_k}] \in \mathbb{R}^{n \times k}$ , where  $k > d$  and  $\mathbf{D}_{i_j} := \mathbf{x}_{i_j} - \mathbf{x}_i$ ,  $j = 1, \dots, k$ .
2. Obtain an orthonormal basis  $\tilde{\mathbf{T}}_i = \{\tilde{\mathbf{t}}_i^{(1)}, \dots, \tilde{\mathbf{t}}_i^{(d)}\}$  for the approximated tangent space  $\widetilde{T_{\mathbf{x}_i} \Gamma}$ , by taking the singular value decomposition (SVD) of  $\mathbf{D}_i$ .

To attain a higher-order approximation of the local tangent space, we consider the Generalized Moving Least Square method [11, 24, 29, 33]. Generally, we use an intrinsic polynomial to approximate smooth function  $g : \Gamma \rightarrow \mathbb{R}$  over the neighborhood of  $\mathbf{x}_i$  which is the optimal solution for the following least-squares problem,

$$\min_{\hat{g} \in \mathbb{P}_{\mathbf{x}_i}^{\ell, d}} \sum_{j=1}^k \left( g(\mathbf{x}_{i_j}) - \hat{g}(\mathbf{x}_{i_j}) \right)^2,$$

where  $\mathbb{P}_{\mathbf{x}_i}^{\ell, d}$  is the space of intrinsic polynomial with degree up to  $\ell$  at the point  $\mathbf{x}_i \in \Gamma \subset \mathbb{R}^d$ . We refer to  $\hat{g}$  as the Generalized Moving Least Squares (GMLS) estimate of  $g$ . For convenience in the discussion below, we present an error bound (cast in our notation) for this least-squares fit, as derived in [24].

**Proposition 3.1.** *Let  $X \subset \Gamma$  be a set of  $N$  uniformly sampled i.i.d. data from a  $d$ -dimensional manifold  $\Gamma$ . Assume that  $g \in C^{\ell+1}(\Gamma)$ . With probability higher than  $1 - \frac{1}{N}$ ,*

$$|D^\alpha g - D^\alpha \hat{g}| = \mathcal{O}\left(\left(\frac{\log N}{N}\right)^{\frac{\ell+1-|\alpha|}{d}}\right),$$

as  $N \rightarrow \infty$ . Here,  $D^\alpha$  denotes the multiindex derivative of order  $|\alpha|$ , and the constant in the big- $\mathcal{O}$  notation can depend on  $d$ , but it is independent of  $N$ .

In the tangent space approximation, the function  $g$  will be the local parameterization of the manifold, with the tangent space represented by its Jacobian. To illustrate the idea, we consider the case  $d = 1$  and  $n = 2$  in our paper. Recall that from the local SVD method, we obtain  $\{\tilde{\mathbf{t}}_i, \tilde{\mathbf{n}}_i\}$ , where  $\tilde{\mathbf{t}}_i$  is the approximate tangent vector at  $\mathbf{x}_i$ , and  $\tilde{\mathbf{n}}_i$  is an approximation of the normal direction at  $\mathbf{x}_i$ . We first project  $\mathbf{D}_i$  onto the estimated tangent space,

$$\tilde{T}(i) = \{\tilde{\mathbf{t}}_i \cdot (\mathbf{x}_{i_1} - \mathbf{x}_{i_1}), \dots, \tilde{\mathbf{t}}_i \cdot (\mathbf{x}_{i_k} - \mathbf{x}_{i_1})\} \subset \widetilde{T_{\mathbf{x}_i}\Gamma},$$

and denote the normal components as

$$\tilde{N}(i) = \{\tilde{\mathbf{n}}_i \cdot (\mathbf{x}_{i_1} - \mathbf{x}_{i_1}), \dots, \tilde{\mathbf{n}}_i \cdot (\mathbf{x}_{i_k} - \mathbf{x}_{i_1})\}.$$

Consider a polynomial  $\tilde{p}_i : \widetilde{T_{\mathbf{x}_i}\Gamma} \rightarrow \mathbb{R}$  defined by

$$\tilde{p}_i(\tilde{s}) = \tilde{\alpha}_{i,1}\tilde{s} + \tilde{\alpha}_{i,2}\tilde{s}^2 + \dots + \tilde{\alpha}_{i,\ell}\tilde{s}^\ell,$$

where  $\tilde{s} \in \tilde{T}(i)$  and the coefficients are obtained by a least squares fit to the data in  $\tilde{T}(i)$  with labels given by  $\tilde{N}(i)$ , i.e.,

$$(\tilde{\alpha}_{i,1}, \dots, \tilde{\alpha}_{i,\ell}) = \operatorname{argmin} \sum_{j=1}^k \left( \tilde{p}_i(\tilde{s}) - \tilde{\mathbf{n}}_i \cdot (\mathbf{x}_{i_j} - \mathbf{x}_{i_1}) \right)^2.$$

Therefore, we can define a local coordinate chart for the manifold near the point  $\mathbf{x}_i$  using the embedding map  $\tilde{\iota}_i : \widetilde{T_{\mathbf{x}_i}\Gamma} \rightarrow \mathbb{R}^2$ ,

$$\tilde{\iota}_i(\tilde{s}) = \mathbf{x}_i + \tilde{\mathbf{t}}_i \tilde{s} + \tilde{\mathbf{n}}_i \tilde{p}_i(\tilde{s}). \quad (3)$$

With this GMLS approximation, we also inherit the estimated tangent space from the Jacobian of  $\tilde{\iota}_i$  defined in (3). The GMLS approximation of the tangent vectors over the neighborhood of  $\mathbf{x}_i$  is

$$\hat{\mathbf{t}}_i(\tilde{s}) = \tilde{\mathbf{t}}_i + \tilde{\mathbf{n}}_i \tilde{p}'_i(\tilde{s}), \quad (4)$$

with the estimated tangent vector at  $\mathbf{x}_i$  denoted by  $\hat{\mathbf{t}}_i = \hat{\mathbf{t}}_i(0)$ , as a GMLS approximation to the underlying tangent vector  $\mathbf{t}(\mathbf{x}_i)$ . We should point out that the additional normal correction term in (4) yields an improved approximation compared to the SVD approximation,  $\tilde{\mathbf{t}}_i$ . For uniformly sampled random data of size  $N$ , it was shown that the SVD approximation converges at order  $N^{-1}$ , provided that a sufficiently large number of  $k$ -nearest points is used (see Remark 9 in [20]). According to Proposition 3.1, if the manifold is  $C^{\ell+1}$ , the GMLS estimate  $\tilde{\iota}_i(0)$  of the true parameterization  $\mathbf{x}_i = \iota(s)$  for some  $s$  has an error of order  $N^{-\ell-1}$ , ignoring the  $\log(N)$  factor. Then the tangent vector estimate  $\hat{\mathbf{t}}_i$  converges at rate  $N^{-\ell}$ , which indicates an improved estimate for  $\ell > 1$  and nonzero  $\tilde{p}'_i(0) = \tilde{\alpha}_{i,1}$ . This fact suggests that the estimation for the local parameterization (as well as the local tangent vector) can be refined by applying the GMLS procedure iteratively on the local coordinates  $(\tilde{\mathbf{t}}_i, \tilde{\mathbf{n}}_i)$ , where  $\tilde{\mathbf{n}}_i$  is a unit normal vector pointing outward from  $\Omega(t)$  such that  $\tilde{\mathbf{t}}_i \cdot \tilde{\mathbf{n}}_i = 0$ . Specifically, the GMLS approximation of the manifold can be repeated near the point  $\mathbf{x}_i$  by employing the embedding map  $\iota_i : T_{\mathbf{x}_i}\Gamma \rightarrow \mathbb{R}^2$ ,

$$\iota_i(s) = \mathbf{x}_i + \hat{\mathbf{t}}_i s + \hat{\mathbf{n}}_i p_i(s), \quad (5)$$

where  $p_i(s) = \alpha_{i,1}s + \alpha_{i,2}s^2 + \dots + \alpha_{i,\ell}s^\ell$  and  $\alpha_{i,1}, \alpha_{i,2}, \dots, \alpha_{i,\ell}$  are obtained via GMLS fitting using the data pairs from  $s \in T(i) = \{\tilde{\mathbf{t}}_i \cdot (\mathbf{x}_{i_1} - \mathbf{x}_{i_1}), \dots, \tilde{\mathbf{t}}_i \cdot (\mathbf{x}_{i_k} - \mathbf{x}_{i_1})\} \subset T_{\mathbf{x}_i}\Gamma$  and  $N(i) = \{\tilde{\mathbf{n}}_i \cdot (\mathbf{x}_{i_1} - \mathbf{x}_{i_1}), \dots, \tilde{\mathbf{n}}_i \cdot (\mathbf{x}_{i_k} - \mathbf{x}_{i_1})\}$ . We iterate this process multiple times, updating tangent vector estimate with the Jacobian of  $\iota_i(0)$ , and stop when the polynomial linear coefficient  $p'_i(0)$  falls below a desired tolerance as a stopping criterion, as further iterations provide negligible improvement. In our numerical simulations, we take this stopping criterion to be  $p'_i(0) = \alpha_{i,1} \approx 10^{-12}$ , and denote the resulting estimated local tangent and normal vectors as  $(\hat{\mathbf{t}}_i, \hat{\mathbf{n}}_i)$  for notational simplicity. As a result,  $p_i(s)$  effectively has no linear term, i.e.,  $p_i(s) = \alpha_{i,2}s^2 + \dots + \alpha_{i,\ell}s^\ell$ . The overall GMLS method is summarized in Algorithm 1.

**Algorithm 1** Generalized Moving Least Squares Approximation for the Local Parametrization

---

**Input:** A set of (distinct) nodes  $X = \{\mathbf{x}_i\}_{i=1}^N \subset \Gamma$ ,  $k (\ll N)$  nearest neighbors of the point  $\mathbf{x}_i$  in the stencil  $K(i) = \{\mathbf{x}_{i_j}\}_{j=1}^k$  and the approximate bases  $\{\tilde{\mathbf{t}}_i, \tilde{\mathbf{n}}_i\}_{i=1}^N$  of the local tangent and normal spaces via the classical local SVD method.

- 1: **for**  $i \in \{1, \dots, N\}$  **do**
- 2:     Construct the matrix  $\Phi \in \mathbb{R}^{k, \ell}$  and the vector  $\Psi \in \mathbb{R}^k$  with

$$\Phi_{j,r} = \left( \tilde{\mathbf{t}}_i \cdot (\mathbf{x}_{i_j} - \mathbf{x}_{i_1}) \right)^r, \quad \Psi_j = \tilde{\mathbf{n}}_i \cdot (\mathbf{x}_{i_j} - \mathbf{x}_{i_1}), \quad j = 1, \dots, k, \quad r = 1, \dots, \ell.$$

- 3:     Obtain the coefficients  $\tilde{\alpha} = [\tilde{\alpha}_{i,1}, \tilde{\alpha}_{i,2}, \dots, \tilde{\alpha}_{i,\ell}]^\top$  of the intrinsic polynomial  $\tilde{p}_i(\tilde{s})$  with

$$\tilde{\alpha} = (\Phi^\top \Phi)^{-1} \Phi^\top \Psi.$$

- 4:     Construct the improved approximation of the local tangent vectors with

$$\hat{\mathbf{t}}_i(\tilde{s}) = \tilde{\mathbf{t}}_i + \tilde{\mathbf{n}}_i \tilde{p}'_i(\tilde{s}),$$

and the estimate local normal vectors  $\hat{\mathbf{n}}_i$  can be constructed by rotating  $\hat{\mathbf{t}}_i$  and choosing the orientation so that it points outward from  $\Omega(t)$ .

- 5:     The following steps improve the estimation, set  $\alpha_{i,1} = \tilde{\alpha}_{i,1}$ .
- 6:     **while**  $p'_i(0) = \alpha_{i,1} > 10^{-12}$  **do**

- 7:         Update the vectors  $\tilde{\mathbf{t}}_i, \tilde{\mathbf{n}}_i \leftarrow \hat{\mathbf{t}}_i, \hat{\mathbf{n}}_i$

Repeat step 2.

Repeat step 3 above with output denoted as  $\alpha = [\alpha_{i,1}, \alpha_{i,2}, \dots, \alpha_{i,\ell}]^\top$  of the intrinsic polynomial  $p_i(s)$  with

$$\alpha = (\Phi^\top \Phi)^{-1} \Phi^\top \Psi.$$

Construct the improved approximation as in Step 4 above, with output

$$\hat{\mathbf{t}}_i(s) = \hat{\mathbf{t}}_i + \hat{\mathbf{n}}_i p'_i(s),$$

and the estimate local normal vectors  $\hat{\mathbf{n}}_i$  can be constructed by rotating  $\hat{\mathbf{t}}_i$  and choosing the orientation so that it points outward from  $\Omega(t)$ .

- 8:     **end while**

- 9:     **end for**

**Output:** The intrinsic polynomial approximation for the local parametrization  $\{p_i(s)\}_{i=1}^N$ .

---

Let  $\gamma_i(s) = (s, p_i(s))$  be the coordinates in (5), which is a local parametric representation of  $\Gamma(t)$  near the point  $\mathbf{x}_i$ . Then, the approximate curvature near the point  $\mathbf{x}_i$  is given by,

$$\kappa_i(s) = -\frac{\det(\gamma', \gamma'')}{\|\gamma'\|^3} = -\frac{p''_i(s)}{\left(1 + (p'_i(s))^2\right)^{\frac{3}{2}}}, \quad (6)$$

with the estimated curvature at  $\mathbf{x}_i$  denoted by  $\kappa_i = \kappa_i(0) = -2\alpha_{i,2}$ . Here we point out that the negative sign in (6) is due to  $\hat{\mathbf{n}}_i$  pointing out of  $\Omega(t)$  (for example,  $\kappa_i = 1$  and  $\alpha_{i,2} < 0$  in the case of a unit circle). According to Proposition 3.1, the GMLS approximation of the curvature converges at rate  $(N^{-1} \log N)^{\ell-1}$  for uniformly sampled random data of size  $N$ . The convergence result for the unit circle case is demonstrated in Figure 1 for  $\ell = 3$  and 4, where the average curvature error is defined as

$$e_\kappa = \sqrt{\frac{1}{N} \sum_{i=1}^N (\kappa_i - 1)^2}. \quad (7)$$

The numerical results suggest that the errors are slightly faster than the theoretical bound by a factor of  $(\log N)^{\ell-1}$  for  $\ell = 3$  and 4.

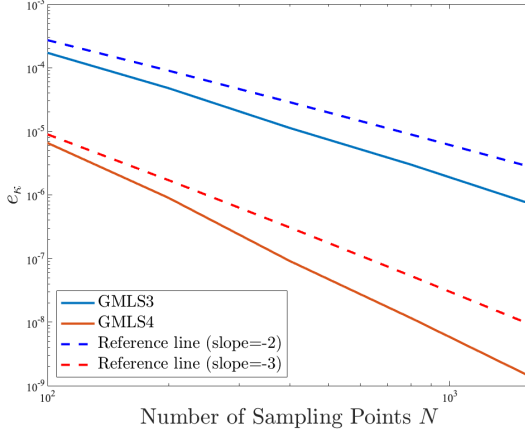


Figure 1: Root-Mean-Square errors of the curvature as defined in (7) as functions of  $N$  for the GMLS estimates with  $\ell = 3$  and 4.

### 3.2 Quadrature rule to approximate the boundary integral equation

In this section, we discretize the BIE (2a) in space, which can be written as a linear system  $AV_n(\mathbf{x}) = b(\mathbf{x})$ , with

$$AV_n(\mathbf{x}) = \int_{\Gamma} G(\mathbf{x}, \mathbf{y}) V_n(\mathbf{y}) dS_{\mathbf{y}}, \quad (8)$$

$$b(\mathbf{x}) = -\frac{\kappa(\mathbf{x})}{2} - \int_{\Gamma} \kappa(\mathbf{y}) \nabla G(\mathbf{x}, \mathbf{y}) \cdot \mathbf{n}(\mathbf{y}) dS_{\mathbf{y}}. \quad (9)$$

We approximate the boundary integral in (8)-(9) with the approximate local chart obtained from the GMLS approximation in (5). Subsequently, we employ a quadrature rule to derive a discrete approximation of the linear system.

Locally, near  $\mathbf{x}_j$ , we approximate

$$dS_{\mathbf{y}} = \sqrt{|\iota'(s)|} ds \approx \sqrt{|\iota'_j(s)|} ds = \sqrt{1 + (p'_j(s))^2} ds, \quad (10)$$

where we use the local parameterization  $\mathbf{y} = \iota_j(s)$  in (5) near  $\mathbf{x}_j$  for all  $j = 1, \dots, N$ . In terms of the local coordinate system through a change of variables, at  $\mathbf{x} = \mathbf{x}_i \in \Gamma(t)$ ,

$$AV_n(\mathbf{x}_i) \approx \int_{\Delta s_{-i}}^{\Delta s_i} G(\mathbf{x}_i, \iota_i(s)) V_n(\iota_i(s)) \sqrt{1 + (p'_i(s))^2} ds + \sum_{j \neq i-1, i} \int_0^{\Delta s_j} G(\mathbf{x}_i, \iota_j(s)) V_n(\iota_j(s)) \sqrt{1 + (p'_j(s))^2} ds, \quad (11)$$

where  $\Delta s_i = \hat{\mathbf{t}}_i^\top (\mathbf{x}_{i+1} - \mathbf{x}_i) > 0$ ,  $\Delta s_{-i} = \hat{\mathbf{t}}_i^\top (\mathbf{x}_{i-1} - \mathbf{x}_i) < 0$ .

Since  $G(\mathbf{x}, \mathbf{y}) = -\frac{1}{2\pi} \ln \|\mathbf{x} - \mathbf{y}\|$ ,

$$G(\mathbf{x}_i, \iota_i(s)) = -\frac{1}{2\pi} \ln \|\mathbf{x}_i - (\mathbf{x}_i + \hat{\mathbf{t}}_i s + \hat{\mathbf{n}}_i p_i(s))\| = -\frac{1}{2\pi} \ln \sqrt{s^2 + p_i^2(s)}, \quad (12)$$

it is clear that the first integral in (11) is singular at  $s = 0$ , because  $\iota_i(0) = \mathbf{x}_i$ . Then we rewrite the first term in (11) as

$$\begin{aligned} \int_{\Delta s_{-i}}^{\Delta s_i} G(\mathbf{x}_i, \iota_i(s)) V_n(\iota_i(s)) \sqrt{1 + (p'_i(s))^2} ds &= \underbrace{-\frac{1}{2\pi} \int_{\Delta s_{-i}}^{\Delta s_i} \ln |s| V_n(\iota_i(s)) \sqrt{1 + (p'_i(s))^2} ds}_{=I_S} \\ &\quad \underbrace{-\frac{1}{4\pi} \int_{\Delta s_{-i}}^{\Delta s_i} \ln \left(1 + \frac{p_i^2(s)}{s^2}\right) V_n(\iota_i(s)) \sqrt{1 + (p'_i(s))^2} ds}_{I_{NS}}. \end{aligned} \quad (13)$$

Notice that  $\frac{p_i(s)}{s} \Big|_{s=0} = 0$ . Thus, (13) has a singular term  $I_S$  that involves  $\ln |s|$ . Accordingly, we can rewrite (11) as

$$AV_n(\mathbf{x}_i) \approx I_S + I_{NS}, \quad (14)$$

where the nonsingular part  $I_N$  consists of  $I_{NS}$  and the second integral term in (11),

$$I_N = I_{NS} + \sum_{j \neq i-1, i} \int_0^{\Delta s_j} G(\mathbf{x}_i, \iota_j(s)) V_n(\iota_j(s)) \sqrt{1 + (p'_j(s))^2} ds, \quad (15)$$

which can be further discretized using any standard quadrature rule.

To handle the singular term  $I_S$ , the function  $\psi_i(s) := V_n(\iota_i(s)) \sqrt{1 + (p'_i(s))^2}$  is approximated by a second-order polynomial expansion  $\tilde{\psi}_i(s) = \beta_0 + \beta_1 s + \beta_2 s^2$  using three interpolation points at  $s = 0$ ,  $s = \Delta s_i$ , and  $s = \Delta s_{-i}$ . This polynomial approximation yields the following system

$$\begin{cases} \tilde{\psi}_i(0) = V_n(\mathbf{x}_i), \\ \tilde{\psi}_i(\Delta s_i) = V_n(\mathbf{x}_{i+1}) \sqrt{1 + (p'_i(\Delta s_i))^2}, \\ \tilde{\psi}_i(\Delta s_{-i}) = V_n(\mathbf{x}_{i-1}) \sqrt{1 + (p'_i(\Delta s_{-i}))^2}, \end{cases} \quad (16)$$

with an explicit solution:

$$\begin{cases} \beta_0 = V_n(\mathbf{x}_i), \\ \beta_1 = V_n(\mathbf{x}_{i+1}) \frac{\Delta s_{-i} \sqrt{1 + (p'_i(\Delta s_i))^2}}{\Delta s_i (\Delta s_{-i} - \Delta s_i)} - V_n(\mathbf{x}_{i-1}) \frac{\Delta s_i \sqrt{1 + (p'_i(\Delta s_{-i}))^2}}{\Delta s_{-i} (\Delta s_{-i} - \Delta s_i)} - V_n(\mathbf{x}_i) \frac{\Delta s_i + \Delta s_{-i}}{\Delta s_i \Delta s_{-i}}, \\ \beta_2 = V_n(\mathbf{x}_{i+1}) \frac{\sqrt{1 + (p'_i(\Delta s_i))^2}}{\Delta s_i (\Delta s_i - \Delta s_{-i})} - V_n(\mathbf{x}_{i-1}) \frac{\sqrt{1 + (p'_i(\Delta s_{-i}))^2}}{\Delta s_{-i} (\Delta s_i - \Delta s_{-i})} + V_n(\mathbf{x}_i) \frac{1}{\Delta s_i \Delta s_{-i}}. \end{cases} \quad (17)$$

Then the singular term  $I_S$  can be approximated by,

$$I_S \approx \tilde{I}_S = -\frac{1}{2\pi} \int_{\Delta s_{-i}}^{\Delta s_i} \beta_0 \ln|s| ds - \frac{1}{2\pi} \int_{\Delta s_{-i}}^{\Delta s_i} \beta_1 s \ln|s| ds - \frac{1}{2\pi} \int_{\Delta s_{-i}}^{\Delta s_i} \beta_2 s^2 \ln|s| ds, \quad (18)$$

where

$$\begin{aligned} -\frac{1}{2\pi} \int_{\Delta s_{-i}}^{\Delta s_i} \beta_0 \ln|s| ds &= -\frac{\beta_0}{2\pi} \left( -\Delta s_{-i} \ln(-\Delta s_{-i}) + \Delta s_{-i} + \Delta s_i \ln(\Delta s_i) - \Delta s_i \right), \\ -\frac{1}{2\pi} \int_{\Delta s_{-i}}^{\Delta s_i} \beta_1 s \ln|s| ds &= -\frac{\beta_1}{2\pi} \left( -\frac{1}{2} (\Delta s_{-i})^2 \ln(-\Delta s_{-i}) + \frac{1}{4} (\Delta s_{-i})^2 + \frac{1}{2} (\Delta s_i)^2 \ln(\Delta s_i) - \frac{1}{4} (\Delta s_i)^2 \right), \\ -\frac{1}{2\pi} \int_{\Delta s_{-i}}^{\Delta s_i} \beta_2 s^2 \ln|s| ds &= -\frac{\beta_2}{2\pi} \left( -\frac{1}{3} (\Delta s_{-i})^3 \ln(-\Delta s_{-i}) + \frac{1}{9} (\Delta s_{-i})^3 + \frac{1}{3} (\Delta s_i)^3 \ln(\Delta s_i) - \frac{1}{9} (\Delta s_i)^3 \right). \end{aligned} \quad (19)$$

with  $\beta_0, \beta_1$ , and  $\beta_2$  given as (17).

Combining (17) and (18) for the singular term  $\tilde{I}_S$  and applying the trapezoidal rule to obtain  $\tilde{I}_N$  as a discrete approximation to the nonsingular term  $I_N$  in (15) for simplicity, we obtain the matrix  $\mathbf{A}$  in the linear system  $\mathbf{A}\tilde{\mathbf{V}}_n = \mathbf{b}$ , which serves as a discrete approximation of  $A V_n(\mathbf{x}) = b(\mathbf{x})$  at  $\mathbf{x}_i, i = 1, \dots, N$ . Here,  $\tilde{\mathbf{V}}_n$  is an approximation to  $\mathbf{V}_n$ , whose  $i$ th component is  $(\tilde{\mathbf{V}}_n)_i = V_n(\mathbf{x}_i)$ .

Specifically, components of  $\mathbf{A}$  are:

$$\begin{aligned}
\mathbf{A}_{i,i} = & -\frac{1}{2\pi} \left( -\Delta s_{-i} \ln(-\Delta s_{-i}) + \Delta s_{-i} + \Delta s_i \ln(\Delta s_i) - \Delta s_i \right) \\
& -\frac{1}{2\pi} \left( \frac{\Delta s_i + \Delta s_{-i}}{\Delta s_i \Delta s_{-i}} \right) \left( -\frac{1}{2} (\Delta s_{-i})^2 \ln(-\Delta s_{-i}) + \frac{1}{4} (\Delta s_{-i})^2 + \frac{1}{2} (\Delta s_i)^2 \ln(\Delta s_i) - \frac{1}{4} (\Delta s_i)^2 \right) \\
& -\frac{1}{2\pi} \left( \frac{1}{\Delta s_i \Delta s_{-i}} \right) \left( -\frac{1}{3} (\Delta s_{-i})^3 \ln(-\Delta s_{-i}) + \frac{1}{9} (\Delta s_{-i})^3 + \frac{1}{3} (\Delta s_i)^3 \ln(\Delta s_i) - \frac{1}{9} (\Delta s_i)^3 \right), \\
\mathbf{A}_{i,i-1} = & \frac{1}{2\pi} \left( \frac{\Delta s_i \sqrt{1 + (p'_i(\Delta s_{-i}))^2}}{\Delta s_{-i}(\Delta s_{-i} - \Delta s_i)} \right) \left( -\frac{1}{2} (\Delta s_{-i})^2 \ln(-\Delta s_{-i}) + \frac{1}{4} (\Delta s_{-i})^2 + \frac{1}{2} (\Delta s_i)^2 \ln(\Delta s_i) - \frac{1}{4} (\Delta s_i)^2 \right) \\
& \frac{1}{2\pi} \left( \frac{\sqrt{1 + (p'_i(\Delta s_{-i}))^2}}{\Delta s_{-i}(\Delta s_i - \Delta s_{-i})} \right) \left( -\frac{1}{3} (\Delta s_{-i})^3 \ln(-\Delta s_{-i}) + \frac{1}{9} (\Delta s_{-i})^3 + \frac{1}{3} (\Delta s_i)^3 \ln(\Delta s_i) - \frac{1}{9} (\Delta s_i)^3 \right) \\
& \frac{1}{4\pi} \ln \left( 1 + \frac{p_i^2(\Delta s_{-i})}{(\Delta s_{-i})^2} \right) \sqrt{1 + (p'_i(\Delta s_{-i}))^2} \frac{\Delta s_{-i}}{2} - G(\mathbf{x}_i, \mathbf{x}_{i-1}) \sqrt{1 + (p'_{i-2}(\Delta s_{i-2}))^2} \frac{\Delta s_{i-2}}{2}, \\
\mathbf{A}_{i,i+1} = & -\frac{1}{2\pi} \left( \frac{\Delta s_{-i} \sqrt{1 + (p'_i(\Delta s_i))^2}}{\Delta s_i(\Delta s_{-i} - \Delta s_i)} \right) \left( -\frac{1}{2} (\Delta s_{-i})^2 \ln(-\Delta s_{-i}) + \frac{1}{4} (\Delta s_{-i})^2 + \frac{1}{2} (\Delta s_i)^2 \ln(\Delta s_i) - \frac{1}{4} (\Delta s_i)^2 \right) \\
& -\frac{1}{2\pi} \left( \frac{\sqrt{1 + (p'_i(\Delta s_i))^2}}{\Delta s_i(\Delta s_i - \Delta s_{-i})} \right) \left( -\frac{1}{3} (\Delta s_{-i})^3 \ln(-\Delta s_{-i}) + \frac{1}{9} (\Delta s_{-i})^3 + \frac{1}{3} (\Delta s_i)^3 \ln(\Delta s_i) - \frac{1}{9} (\Delta s_i)^3 \right) \\
& -\frac{1}{4\pi} \ln \left( 1 + \frac{p_i^2(\Delta s_i)}{(\Delta s_i)^2} \right) \sqrt{1 + (p'_i(\Delta s_i))^2} \frac{\Delta s_i}{2} - G(\mathbf{x}_i, \mathbf{x}_{i+1}) \frac{\Delta s_{i+1}}{2}, \\
\mathbf{A}_{i,j} = & G(\mathbf{x}_i, \mathbf{x}_j) \frac{\Delta s_j}{2} - G(\mathbf{x}_i, \mathbf{x}_j) \sqrt{1 + (p'_{j-1}(\Delta s_{j-1}))^2} \frac{\Delta s_{j-1}}{2}, \quad j \neq i-1, i, i+1.
\end{aligned}$$

Next, we formulate  $\mathbf{b}$  which is the discrete approximation of  $b(\mathbf{x})$  in (9), where  $\nabla G(\mathbf{x}, \mathbf{y}) = \frac{1}{2\pi} \frac{\mathbf{x} - \mathbf{y}}{\|\mathbf{x} - \mathbf{y}\|^2}$ . Similarly, we approximate  $b(\mathbf{x}_i)$  with the local parameterized volume in (10) and write the integral in terms of the local coordinate system through a change of variables,

$$\begin{aligned}
b(\mathbf{x}_i) \approx & -\frac{\kappa(\mathbf{x}_i)}{2} - \frac{1}{2} \left[ \int_{\Delta s_{-i}}^{\Delta s_i} \kappa(\iota_i(s)) \cdot (\nabla G(\mathbf{x}_i, \iota_i(s)) \cdot \hat{\mathbf{n}}(\iota_i(s))) \sqrt{1 + (p'_i(s))^2} ds \right. \\
& \left. + \sum_{j \neq i} \int_{\Delta s_{-j}}^{\Delta s_j} \kappa(\iota_j(s)) (\nabla G(\mathbf{x}_i, \iota_j(s)) \cdot \hat{\mathbf{n}}(\iota_j(s))) \sqrt{1 + (p'_j(s))^2} ds \right], \tag{20}
\end{aligned}$$

which can be further discretized using any standard quadrature rule. Notice that the first integral has a singularity when  $s = 0$ , because  $\iota_i(0) = \mathbf{x}_i$ .

To handle the singularity, we calculate  $\nabla G(\mathbf{x}_i, \iota_i(s)) \cdot \hat{\mathbf{n}}(\iota_i(s))|_{s=0}$ . We first derive the unit outer normal vector  $\hat{\mathbf{n}}(\iota_i(s))$  for the points in the neighborhood of  $\mathbf{x}_i$ . Since the unit tangent vector is given as,

$$\hat{\mathbf{t}}(\iota_i(s)) = \frac{\hat{\mathbf{t}}_i + \hat{\mathbf{n}}_i p'_i(s)}{\sqrt{1 + (p'_i(s))^2}}.$$

then the unit outer normal vector for the points in the neighborhood of  $\mathbf{x}_i$  is

$$\hat{\mathbf{n}}(\iota_i(s)) = \text{sign}(p''_i(s)) \frac{\frac{d\hat{\mathbf{t}}(\iota_i(s))}{ds}}{\left\| \frac{d\hat{\mathbf{t}}(\iota_i(s))}{ds} \right\|} = \text{sign}(p''_i(s)) \frac{\hat{\mathbf{n}}_i p''_i(s) - \hat{\mathbf{t}}_i p'_i(s) p''_i(s)}{\sqrt{(p''_i(s))^2 (1 + (p'_i(s))^2)}},$$

where  $\text{sign}(p''_i(s))$  ensures that the unit outer normal vector points outward from  $\Omega(t)$ .

Substitute  $\hat{\mathbf{n}}(\iota_i(s))$  into  $\nabla G(\mathbf{x}_i, \iota_i(s)) \cdot \hat{\mathbf{n}}(\iota_i(s))$ , we have

$$\left. \left( \nabla G(\mathbf{x}_i, \iota_i(s)) \cdot \hat{\mathbf{n}}(\iota_i(s)) \right) \right|_{s=0} = \frac{1}{2\pi} \frac{-s\hat{\mathbf{t}}_i - p_i(s)\hat{\mathbf{n}}_i}{s^2 + p_i^2(s)} \cdot \hat{\mathbf{n}}(\iota_i(s)) \Big|_{s=0} = \frac{\alpha_{i,2}}{2\pi},$$

where we have used the fact that  $p_i(s) = \alpha_{i,2}s^2 + \dots + \alpha_{i,\ell}s^\ell$  for  $\ell \geq 2$ .

For example, applying the trapezoidal rule to (20) for simplicity, we obtain the vector  $\mathbf{b}$  as follows,

$$\begin{aligned} \mathbf{b}_i = & -\frac{\kappa(\mathbf{x}_i)}{2} + \left( \kappa(\mathbf{x}_{i-1}) \left( \nabla G(\mathbf{x}_i, \mathbf{x}_{i-1}) \cdot \hat{\mathbf{n}}_{i-1} \right) \sqrt{1 + (p_i'(\Delta s_{i-1}))^2} + \kappa(\mathbf{x}_i) \frac{\alpha_{i,2}}{2\pi} \right) \frac{\Delta s_{i-1}}{2} \\ & - \left( \kappa(\mathbf{x}_i) \frac{\alpha_{i,2}}{2\pi} + \kappa(\mathbf{x}_{i+1}) \left( \nabla G(\mathbf{x}_i, \mathbf{x}_{i+1}) \cdot \hat{\mathbf{n}}_{i+1} \right) \sqrt{1 + (p_i'(\Delta s_i))^2} \right) \frac{\Delta s_i}{2} \\ & - \sum_{j \neq i-1, i} \left( \kappa(\mathbf{x}_j) \left( \nabla G(\mathbf{x}_i, \mathbf{x}_j) \cdot \hat{\mathbf{n}}_j \right) + \kappa(\mathbf{x}_{j+1}) \left( \nabla G(\mathbf{x}_i, \mathbf{x}_{j+1}) \cdot \hat{\mathbf{n}}_{j+1} \right) \sqrt{1 + (p_j'(\Delta s_j))^2} \right) \frac{\Delta s_j}{2}. \end{aligned}$$

Finally, we solve the linear system  $\mathbf{AV}_n = \mathbf{b}$  to obtain the velocity in the normal direction  $\mathbf{V}_n$ .

### 3.3 Time discretization

Now we apply two time discretization schemes to (2b),  $\frac{d\mathbf{x}}{dt} = \tilde{\mathbf{V}}_n \hat{\mathbf{n}}$  with  $\tilde{\mathbf{V}}_n = \mathbf{A}^{-1}\mathbf{b}$ . For example, we will consider the standard forward Euler scheme and the second-order Runge-Kutta scheme. Denoting the time-discretization with a superscript  $m$ , that is  $\mathbf{x}^m$  as an approximation to  $\mathbf{x}(t_m)$  with time discretization  $\Delta t = t_m - t_{m-1}$ , we have:

**Scheme 3.1** (Forward Euler).

$$\mathbf{x}^{m+1} = \mathbf{x}^m + \Delta t(\tilde{\mathbf{V}}_n)^m \hat{\mathbf{n}}(\mathbf{x}^m).$$

**Scheme 3.2** (Second-order Runge-Kutta).

$$\mathbf{x}^{m+\frac{1}{2}} = \mathbf{x}^m + \frac{\Delta t}{2}(\tilde{\mathbf{V}}_n)^m \hat{\mathbf{n}}(\mathbf{x}^m), \quad (\tilde{\mathbf{V}}_n)^{m+\frac{1}{2}} = \left( \mathbf{A}^{-1} \right)^{m+\frac{1}{2}} \mathbf{b}^{m+\frac{1}{2}}, \quad \mathbf{x}^{m+1} = \mathbf{x}^m + \Delta t(\tilde{\mathbf{V}}_n)^{m+\frac{1}{2}} \hat{\mathbf{n}}(\mathbf{x}^{m+\frac{1}{2}}).$$

## 4 Error analysis

In this section, we provide an error analysis for the discrete approximation of the boundary integral  $AV_n(\mathbf{x}) = b(\mathbf{x})$  on the data set  $\{\mathbf{x}_i\}_{i=1,\dots,N} \subset \Gamma(t)$  for a fixed time  $t \geq 0$ . In the following discussion, we will first deduce some technical results to be used for achieving the consistency of the discrete approximation of  $AV_n(\mathbf{x}_i)$  and  $b(\mathbf{x}_i)$ .

**Proposition 4.1.**  *$X = \{\mathbf{x}_i\}_{i=1,\dots,N} \subset \Gamma(t)$  are randomly sampled from a uniform distribution of a 1-dimensional smooth,  $C^{\ell+1}$ , boundary  $\Gamma(t)$  (closed curve) at a fixed time  $t \geq 0$ . We denote  $\mathbf{x}_{i-1}$  and  $\mathbf{x}_{i+1}$  to be the two adjacent points to  $\mathbf{x}_i$  on the boundary curve  $\Gamma(t)$  for all  $i = 1, \dots, N$ , with periodic structure, that is,  $\mathbf{x}_{N+1} = \mathbf{x}_1$  and  $\mathbf{x}_0 = \mathbf{x}_N$ . Suppose that we parameterize  $\Gamma(t)$  locally at  $\mathbf{x}_i$  with  $p_i \in C^\ell(\mathbb{R})$  using Algorithm 1. Then, with probability higher than  $1 - \frac{2}{N}$ ,*

$$|\Delta s_i - \Delta s(\mathbf{x}_i)| = \mathcal{O}\left(\left(\frac{\log N}{N}\right)^{\ell+1}\right), \quad (21)$$

and with probability higher than  $1 - \frac{1}{N}$ ,

$$\left| dS_{\mathbf{y}} - \sqrt{1 + (p_j'(s))^2} ds \right| = \mathcal{O}\left(\left(\frac{\log N}{N}\right)^\ell\right), \quad (22)$$

as  $N \rightarrow \infty$ .

*Proof.* Suppose that  $X = \{\mathbf{x}_i\}_{i=1,\dots,N} \subset \Gamma(t)$  are randomly sampled from a uniform distribution. We denote the  $\mathbf{x}_{i-1}$  and  $\mathbf{x}_{i+1}$  to be the two adjacent points to  $\mathbf{x}_i$  on the boundary curve  $\Gamma(t)$  for all  $i = 1, \dots, N$ , with periodic structure, that is,  $\mathbf{x}_{N+1} = \mathbf{x}_1$  and  $\mathbf{x}_0 = \mathbf{x}_N$ . In such a configuration, it is easy to see that,

$$\max_i \frac{1}{2} d_g(\mathbf{x}_i, \mathbf{x}_{i+1}) = \sup_{\mathbf{x} \in \Gamma(t)} \min_i d_g(\mathbf{x}, \mathbf{x}_i) = h_{X, \Gamma},$$

which is known as the fill distance or sometimes regarded as the mesh size. For uniform random samples, it is known that (see Lemma B.2 in [20]) with probability higher than  $1 - \frac{1}{N}$ ,  $h_{X,\Gamma} = \mathcal{O}(N^{-1} \log(N))$  as  $N \rightarrow \infty$ . Let  $h = d_g(\mathbf{x}_{i+1}, \mathbf{x}_i)$ , one can show that

$$\|\mathbf{x}_{i+1} - \mathbf{x}_i\| = h + \mathcal{O}(h^3),$$

as  $N \rightarrow \infty$  (see Lemma 6 in [3] or the proof of Proposition 3.1 in [23]). Together, we have that with probability higher than  $1 - \frac{1}{N}$ ,

$$\max_i \|\mathbf{x}_{i+1} - \mathbf{x}_i\| = 2h_{X,\Gamma} + \mathcal{O}(h_{X,\Gamma}^3) = \mathcal{O}\left(\frac{\log N}{N}\right), \quad (23)$$

as  $N \rightarrow \infty$ . Moreover, by Proposition 3.1, the tangent vector estimate  $\hat{\mathbf{t}}_i$  of the underlying tangent vector  $\mathbf{t}(\mathbf{x}_i)$  converges at rate  $(N^{-1} \log N)^\ell$ , with probability higher than  $1 - \frac{2}{N}$ ,

$$|\Delta s_i - \Delta s(\mathbf{x}_i)| = |\hat{\mathbf{t}}_i^\top (\mathbf{x}_{i+1} - \mathbf{x}_i) - \mathbf{t}(\mathbf{x}_i)^\top (\mathbf{x}_{i+1} - \mathbf{x}_i)| \leq \|\hat{\mathbf{t}}_i - \mathbf{t}(\mathbf{x}_i)\| \|\mathbf{x}_{i+1} - \mathbf{x}_i\| = \mathcal{O}\left(\left(\frac{\log N}{N}\right)^{\ell+1}\right),$$

as  $N \rightarrow \infty$ .

Also, from  $dS_y = \sqrt{|\iota'(s)|} ds \approx \sqrt{1 + (p'_j(s))^2} ds$ , one can verify that

$$\left| \sqrt{\hat{\mathbf{t}}_i^\top \hat{\mathbf{t}}_i} - \sqrt{\mathbf{t}(\mathbf{x}_i)^\top \mathbf{t}(\mathbf{x}_i)} \right| = \left| \frac{\hat{\mathbf{t}}_i^\top \hat{\mathbf{t}}_i - \mathbf{t}(\mathbf{x}_i)^\top \mathbf{t}(\mathbf{x}_i)}{\sqrt{\hat{\mathbf{t}}_i^\top \hat{\mathbf{t}}_i + \sqrt{\mathbf{t}(\mathbf{x}_i)^\top \mathbf{t}(\mathbf{x}_i)}}} \right| = \left| \frac{(\mathbf{t}(\mathbf{x}_i) + \hat{\mathbf{t}}_i)^\top (\hat{\mathbf{t}}_i - \mathbf{t}(\mathbf{x}_i))}{\sqrt{\hat{\mathbf{t}}_i^\top \hat{\mathbf{t}}_i + 1}} \right| = \mathcal{O}\left(\left(\frac{\log N}{N}\right)^\ell\right).$$

□

Now we study the consistency of our approximation to  $AV_n(\mathbf{x}) = \int_\Gamma G(\mathbf{x}, \mathbf{y}) V_n(\mathbf{y}) dS_y$  at each  $\mathbf{x}_i$ . To make the discussion concise, we define

$$AV_n(\mathbf{x}_i) = I_S^* + I_N^*,$$

where

$$\begin{aligned} I_S^* &= -\frac{1}{2\pi} \int_{\Delta s(\mathbf{x}_{-i})}^{\Delta s(\mathbf{x}_i)} \ln|s| V_n(\iota(s)) \sqrt{|\iota'(s)|} ds, \\ I_N^* &= -\frac{1}{4\pi} \int_{\Delta s(\mathbf{x}_{-i})}^{\Delta s(\mathbf{x}_i)} \ln\left(1 + \frac{p^2(s)}{s^2}\right) V_n(\iota(s)) \sqrt{|\iota'(s)|} ds + \sum_{j \neq i-1, i} \int_0^{\Delta s(\mathbf{x}_j)} G(\mathbf{x}_i, \iota(s)) V_n(\iota(s)) \sqrt{|\iota'(s)|} ds, \end{aligned}$$

with  $p(s)$  representing the true parameterization of the boundary curve. The proposition below follows from estimating the errors in approximating these integrals by  $\tilde{I}_S$ , the approximation to  $I_S$  in (18), and  $\tilde{I}_N$ , the quadrature (e.g., Newton's Cotes family) approximation to  $I_N$  in (15).

**Proposition 4.2.** *Assume that the assumptions of Proposition 3.1 and Proposition 4.1 hold. In addition, we also assume that  $V_n \in C^3(\Gamma)$ . Then, with probability higher than  $1 - \frac{23}{N}$ ,*

$$|AV_n(\mathbf{x}_i) - (\mathbf{AV}_n)_i| \leq |I_S^* - \tilde{I}_S| + |I_N^* - \tilde{I}_N| = \mathcal{O}\left(\frac{(\log N)^{\ell+2}}{N^{\ell-2}}\right) + \mathcal{O}\left(\left(\frac{\log N}{N}\right)^q\right),$$

as  $N \rightarrow \infty$ . Here, we denote  $\tilde{I}_N$  to be the quadrature approximation to  $I_N$  in (15) of order  $q$ , and  $\tilde{I}_S$  as the approximation in (18) to  $I_S$  in (13).

*Proof.* Note that

$$\begin{aligned} |I_S^* - \tilde{I}_S| &\leq |I_S^* - I_S| + |I_S - \tilde{I}_S| \\ &= \frac{1}{2\pi} \left| \int_{\Delta s(\mathbf{x}_{-i})}^{\Delta s(\mathbf{x}_i)} \ln|s| \psi^*(s) ds - \int_{\Delta s_{-i}}^{\Delta s_i} \ln|s| \psi_i(s) ds \right| + \frac{1}{2\pi} \left| \int_{\Delta s_{-i}}^{\Delta s_i} \ln|s| \psi_i(s) ds - \int_{\Delta s_{-i}}^{\Delta s_i} \ln|s| \tilde{\psi}_i(s) ds \right| \end{aligned} \quad (24)$$

where  $\tilde{\psi}_i = \beta_0 + \beta_1 s + \beta_2 s^2$  denotes the second-order polynomial approximation to  $\psi_i(s) := V_n(\iota_i(s)) \sqrt{1 + (p'_i(s))^2}$  as discussed in (16) and we have defined  $\psi^*(s) := V_n(\iota(s)) \sqrt{|\iota'(s)|}$  to simplify the notation.

By (22), Proposition 3.1 and Proposition 4.1, with probability higher than  $1 - \frac{2}{N}$ ,

$$\begin{aligned} |\psi^*(s) - \psi_i(s)| &\leq |V_n(\iota(s))| \left| \sqrt{|\iota'(s)|} - \sqrt{1 + (p'_i(s))^2} \right| + \sqrt{1 + (p'_i(s))^2} |V_n(\iota(s)) - V_n(\iota_i(s))| \\ &\leq \mathcal{O}\left(\left(\frac{\log N}{N}\right)^\ell\right) + C|\iota(s) - \iota_i(s)| = \mathcal{O}\left(\left(\frac{\log N}{N}\right)^\ell\right) + \mathcal{O}\left(\left(\frac{\log N}{N}\right)^{\ell+1}\right) = \mathcal{O}\left(\left(\frac{\log N}{N}\right)^\ell\right). \end{aligned} \quad (25)$$

Then the first error term in (24) can be bounded as follows,

$$\begin{aligned} \left| \int_{\Delta s(\mathbf{x}_{-i})}^{\Delta s(\mathbf{x}_i)} \ln|s| \psi^*(s) ds - \int_{\Delta s_{-i}}^{\Delta s_i} \ln|s| \psi_i(s) ds \right| &\leq \left| \int_{\Delta s(\mathbf{x}_{-i})}^{\Delta s(\mathbf{x}_i)} \ln|s| \psi^*(s) ds - \int_{\Delta s_{-i}}^{\Delta s_i} \ln|s| \psi^*(s) ds \right| \\ &\quad + \left| \int_{\Delta s_{-i}}^{\Delta s_i} \ln|s| (\psi^*(s) - \psi_i(s)) ds \right| \\ &\leq C(|\Delta s_i - \Delta s(\mathbf{x}_i)| + |\Delta s_{-i} - \Delta s(\mathbf{x}_{-i})|) \\ &\quad + \max_{s \in [\Delta s_{-i}, \Delta s_i]} |\psi^*(s) - \psi_i(s)| \left| \int_{\Delta s_{-i}}^{\Delta s_i} \ln|s| ds \right| \\ &= \mathcal{O}\left(\left(\frac{\log N}{N}\right)^{\ell+1}\right) + \mathcal{O}\left(\left(\frac{\log N}{N}\right)^{\ell+1} \ln\left(\frac{\log N}{N}\right)\right) \\ &= \mathcal{O}\left(\left(\frac{\log N}{N}\right)^{\ell+1} \ln\left(\frac{\log N}{N}\right)\right), \end{aligned}$$

with probability higher than  $1 - \frac{7}{N}$ , where we used the bounds from Proposition 4.1.

The second error term in (24) is bounded by the quadratic interpolation error of the integrand,

$$\begin{aligned} \left| \int_{\Delta s_{-i}}^{\Delta s_i} \ln|s| \psi_i(s) ds - \int_{\Delta s_{-i}}^{\Delta s_i} \ln|s| \tilde{\psi}_i(s) ds \right| &\leq \max_{s \in [\Delta s_{-i}, \Delta s_i]} |\psi_i(s) - \tilde{\psi}_i(s)| \left| \int_{\Delta s_{-i}}^{\Delta s_i} \ln|s| ds \right| \\ &\leq Ch_{X,\Gamma}^3 (\Delta s_i \ln(\Delta s_i) - \Delta s_{-i} \ln(-\Delta s_{-i})) \\ &= \mathcal{O}\left(\left(\frac{\log N}{N}\right)^4 \ln\left(\frac{\log N}{N}\right)\right), \end{aligned}$$

with probability higher than  $1 - \frac{2}{N}$  for some constant  $C$ , under the assumption that  $\psi_i$  is  $C^3$ .

Asserting the rates in these bounds to (24) and accounting for all probabilities, we obtain

$$|I_S^* - \tilde{I}_S| = \mathcal{O}\left(\left(\frac{\log N}{N}\right)^{\ell+1} \ln\left(\frac{\log N}{N}\right)\right) + \mathcal{O}\left(\left(\frac{\log N}{N}\right)^4 \ln\left(\frac{\log N}{N}\right)\right) \quad (26)$$

with probability higher than  $1 - \frac{9}{N}$ .

Next we consider the error bound for  $|I_N^* - \tilde{I}_N|$ ,

$$\begin{aligned} |I_N^* - \tilde{I}_N| &\leq |I_N^* - I_N| + |I_N - \tilde{I}_N| \\ &= \frac{1}{4\pi} \left| \int_{\Delta s(\mathbf{x}_{-i})}^{\Delta s(\mathbf{x}_i)} \ln\left(1 + \frac{p^2(s)}{s^2}\right) \psi^*(s) ds - \int_{\Delta s_{-i}}^{\Delta s_i} \ln\left(1 + \frac{p_i^2(s)}{s^2}\right) \psi_i(s) ds \right| \\ &\quad + \sum_{j \neq i, i-1} \left| \int_0^{\Delta s(\mathbf{x}_j)} G(\mathbf{x}_i, \iota(s)) \psi^*(s) ds - \int_0^{\Delta s_j} G(\mathbf{x}_i, \iota_j(s)) \psi_j(s) ds \right| + \mathcal{O}\left(\left(\frac{\log N}{N}\right)^q\right), \end{aligned}$$

where  $\tilde{I}_N$  is the quadrature rule approximation to  $I_N$  with error of order  $q$ .

By Proposition 3.1 and (25), we note the following bounds for the integrands. With probability higher than  $1 - \frac{3}{N}$ ,

$$\begin{aligned}
|\varphi^*(s) - \varphi_i(s)| &:= \left| \ln \left( 1 + \frac{p^2(s)}{s^2} \right) \psi^*(s) - \ln \left( 1 + \frac{p_i^2(s)}{s^2} \right) \psi_i(s) \right| \\
&\leq \left| \ln \left( 1 + \frac{p^2(s)}{s^2} \right) \psi^*(s) - \ln \left( 1 + \frac{p_i^2(s)}{s^2} \right) \psi^*(s) \right| \\
&\quad + \left| \ln \left( 1 + \frac{p_i^2(s)}{s^2} \right) \psi^*(s) - \ln \left( 1 + \frac{p_i^2(s)}{s^2} \right) \psi_i(s) \right| \\
&= \left| \frac{1}{1 + p^2(s)/s^2} \right| \left| \frac{p^2(s) - p_i^2(s)}{s^2} \right| |\psi^*(s)| + \mathcal{O} \left( \left( \frac{\log N}{N} \right)^\ell \right) \\
&= \mathcal{O} \left( \frac{(\log N)^{\ell+1}}{N^{\ell-3}} \right),
\end{aligned}$$

where we have used a lower bound for the separation distance,  $|s| \geq \min_{i \neq j} d_g(\mathbf{x}_i, \mathbf{x}_j) = q_{X, \Gamma} \geq N^{-2}$  with probability higher than  $1 - \frac{1}{N}$  (see Lemma A.2 in [37] for the detailed proof).

Similarly, for  $j \neq i, i-1$ , with probability higher than  $1 - \frac{3}{N}$ ,

$$\begin{aligned}
|G(\mathbf{x}_i, \iota(s))\psi^*(s) - G(\mathbf{x}_i, \iota_j(s))\psi_j(s)| &\leq |G(\mathbf{x}_i, \iota(s)) - G(\mathbf{x}_i, \iota_j(s))| |\psi^*(s)| + |G(\mathbf{x}_i, \iota_j(s))| |\psi^*(s) - \psi_j(s)| \\
&= \frac{1}{2\pi} \frac{|(\mathbf{x}_i - \iota(s)) \cdot (\iota(s) - \iota_j(s))|}{\|\mathbf{x}_i - \iota(s)\|^2} |\psi^*(s)| + \mathcal{O} \left( \left( \frac{\log N}{N} \right)^\ell \right) \\
&= \mathcal{O} \left( \frac{(\log N)^{\ell+1}}{N^{\ell-1}} \right).
\end{aligned}$$

Then, one can deduce that with probability higher than  $1 - \frac{8}{N}$ ,

$$\begin{aligned}
\left| \int_{\Delta s(\mathbf{x}_{-i})}^{\Delta s(\mathbf{x}_i)} \varphi^*(s) ds - \int_{\Delta s_{-i}}^{\Delta s_i} \varphi_i(s) ds \right| &\leq \left| \int_{\Delta s(\mathbf{x}_{-i})}^{\Delta s(\mathbf{x}_i)} \varphi^*(s) ds - \int_{\Delta s_{-i}}^{\Delta s_i} \varphi^*(s) ds \right| + \left| \int_{\Delta s_{-i}}^{\Delta s_i} (\varphi^*(s) ds - \varphi_i(s) ds) \right| \\
&\leq C(|\Delta s_i - \Delta s(\mathbf{x}_i)| + |\Delta s_{-i} - \Delta s(\mathbf{x}_{-i})|) + \max_{s \in [\Delta s_{-i}, \Delta s_i]} |\varphi^*(s) - \varphi_i(s)| |\Delta s_i - \Delta s_{-i}| \\
&= \mathcal{O} \left( \left( \frac{\log N}{N} \right)^{\ell+1} \right) + \mathcal{O} \left( \frac{(\log N)^{\ell+2}}{N^{\ell-2}} \right),
\end{aligned}$$

and with probability higher than  $1 - \frac{6}{N}$ ,

$$\left| \int_0^{\Delta s(\mathbf{x}_j)} G(\mathbf{x}_i, \iota(s))\psi^*(s) ds - \int_0^{\Delta s_j} G(\mathbf{x}_i, \iota_j(s))\psi_j(s) ds \right| = \mathcal{O} \left( \left( \frac{\log N}{N} \right)^{\ell+1} \right) + \mathcal{O} \left( \frac{(\log N)^{\ell+2}}{N^\ell} \right).$$

Therefore, with probability higher than  $1 - \frac{14}{N}$ ,

$$\begin{aligned}
|I_N^* - I_N| &\leq \left| \int_{\Delta s(\mathbf{x}_{-i})}^{\Delta s(\mathbf{x}_i)} \varphi^*(s) ds - \int_{\Delta s_{-i}}^{\Delta s_i} \varphi_i(s) ds \right| + \sum_{j \neq i, i-1} \left| \int_0^{\Delta s(\mathbf{x}_j)} G(\mathbf{x}_i, \iota(s))\psi^*(s) ds - \int_0^{\Delta s_j} G(\mathbf{x}_i, \iota_j(s))\psi_j(s) ds \right| \\
&= \mathcal{O} \left( \frac{(\log N)^{\ell+2}}{N^{\ell-2}} \right) + (N-2) \mathcal{O} \left( \frac{(\log N)^{\ell+2}}{N^\ell} \right) \\
&= \mathcal{O} \left( \frac{(\log N)^{\ell+2}}{N^{\ell-2}} \right).
\end{aligned}$$

Finally, we have

$$|I_N^* - \tilde{I}_N| \leq |I_N^* - I_N| + |I_N - \tilde{I}_N| = \mathcal{O} \left( \frac{(\log N)^{\ell+2}}{N^{\ell-2}} \right) + \mathcal{O} \left( \left( \frac{\log N}{N} \right)^q \right). \quad (27)$$

With the bounds in (26) and (27), the proof is completed.  $\square$

Next, we report the consistency of our approximation to (9). See Appendix A for the detailed proof, which follows the same strategy as the proof above.

**Proposition 4.3.** *Let the assumptions of Proposition 3.1 and Proposition 4.1 be valid. Then, with probability higher than than  $1 - \frac{10}{N}$ ,*

$$|b(\mathbf{x}_i) - \mathbf{b}_i| = \mathcal{O}\left(\frac{(\log N)^{\ell+2}}{N^{\ell-2}}\right) + \mathcal{O}\left(\left(\frac{\log N}{N}\right)^q\right),$$

as  $N \rightarrow \infty$ , where  $q$  denotes the quadrature rule error rate.

In the following, we verify the invertibility (and stability) of the estimator  $\mathbf{A}$  of the linear system  $\mathbf{AV}_n = \mathbf{b}$  that will be numerically solved. In this context, recall that  $(\mathbf{V}_n)_i = V_n(\mathbf{x}_i)$ . Our approach will be based on the following result.

**Proposition 4.4** (McLean [32].) *The operator  $A$  as defined in (8) is self-adjoint and coercive under the inner product induced by the Hilbert space,*

$$H_* = \left\{ v \in L^2(\Gamma) \mid \langle v, 1 \rangle = \int_{\Gamma} v(\mathbf{x}) dS_{\mathbf{x}} = 0 \right\}.$$

*The coercivity can be expressed as follows. For all function  $v \in H_*$ ,*

$$\langle v, Av \rangle = \int_{\Gamma} v(\mathbf{x}) Av(\mathbf{x}) dS_{\mathbf{x}} \geq \zeta \|v\|_{L^2(\Gamma)}^2,$$

where  $\zeta > 0$  denotes the coercivity constant.

With this result, we now state the invertibility and positivity condition for the matrix  $\mathbf{A}$ .

**Proposition 4.5.** *Let the assumptions in Proposition 4.2 to be valid. With probability higher than  $1 - \frac{25}{N}$ , the matrix  $\mathbf{A}$  is invertible when the coercivity constant of  $A$ ,*

$$\zeta > C^{-1}(\log N)^{-1} \bar{\delta}(N),$$

for some constant  $C > 0$ , and,

$$\bar{\delta}(N) = \mathcal{O}\left(\frac{(\log N)^{\ell+2}}{N^{\ell-\frac{3}{2}}}\right) + \mathcal{O}\left(\left(\frac{\log(N)}{N}\right)^{\frac{1}{2}}\right)$$

which decays to zero as  $N \rightarrow \infty$ .

*Proof.* Let  $\{\eta_i(\mathbf{x})\}_{i=1}^n$  be linear hat functions defined on a parameterization  $\iota: I \subset \mathbb{R} \rightarrow \Gamma$  such that  $\iota(s) = \mathbf{x}$ . That is, for all  $\mathbf{x}_i \in \Gamma$ ,

$$\eta_i(\mathbf{x}) = \eta_i(\iota(s)) = \begin{cases} \frac{s - s_{i-1}}{s_i - s_{i-1}}, & \text{for } s \in [\iota^{-1}(\mathbf{x}_{i-1}), \iota^{-1}(\mathbf{x}_i)] \\ \frac{s_{i+1} - s}{s_{i+1} - s_i}, & \text{for } s \in [\iota^{-1}(\mathbf{x}_i), \iota^{-1}(\mathbf{x}_{i+1})] \end{cases}.$$

For any  $V_n \in L^2(\Gamma)$ , we can write

$$V_n(\mathbf{x}) = \sum_{i=1}^N V_n(\mathbf{x}_i) \eta_i(\mathbf{x}).$$

To be in  $H^*$ , we require that  $V_n(\mathbf{x}_i)$  satisfies,

$$\sum_{i=1}^N V_n(\mathbf{x}_i) m_i = 0, \quad m_i = \int_{\Gamma} \eta_i(\mathbf{x}) dS_{\mathbf{x}},$$

which is obtained by imposing the *discrete zero-mean constraint*. Then,

$$\zeta \langle V_n, V_n \rangle = \zeta \sum_{i,j=1,\dots,N} V_n(\mathbf{x}_i) V_n(\mathbf{x}_j) \int_{\Gamma} \eta_i(\mathbf{x}) \eta_j(\mathbf{x}) dS_{\mathbf{x}} = \zeta \mathbf{V}_n^T \mathbf{M} \mathbf{V}_n \geq \zeta \lambda_{\min}(\mathbf{M}) \|\mathbf{V}_n\|^2, \quad (28)$$

where

$$\mathbf{M}_{ij} = \int_{\Gamma} \eta_i(\mathbf{x}) \eta_j(\mathbf{x}) dS_{\mathbf{x}},$$

which is SPD. Letting  $\iota(s) = \mathbf{x}_0 + \mathbf{t}(\mathbf{x}_0)s + \mathbf{n}(\mathbf{x}_0)p(s)$ , denoting a parameterization of  $\Gamma$  at  $\mathbf{x}_0$ , one can write

$$\begin{aligned} \mathbf{M}_{ij} &= \int_{\iota^{-1}(\Gamma)} \eta_i(\iota(s)) \eta_j(\iota(s)) \sqrt{1 + (p'(s))^2} \chi_{\{\eta_i(\Gamma) \cap \eta_j(\Gamma) \neq 0\}}(s) ds \\ &\geq \mathbf{L}_{ij} = \int_{\iota^{-1}(\{\eta_i(\Gamma) \cap \eta_j(\Gamma) \neq 0\})} \eta_i(\iota(s)) \eta_j(\iota(s)) ds \geq \int_{-q_{X,\Gamma}}^{q_{X,\Gamma}} \eta_i(\iota(s)) \eta_j(\iota(s)) ds = \begin{cases} \frac{2}{3} q_{X,\Gamma} & \text{if } i = j \\ \frac{1}{4} q_{X,\Gamma} & \text{if } |i - j| = 1, \\ 0, & \text{otherwise.} \end{cases} \end{aligned} \quad (29)$$

where  $q_{X,\Gamma} = \min_{i,j} d_g(\mathbf{x}_i, \mathbf{x}_j)$  denotes the separation distance. It is easy to check that  $\mathbf{M} - \mathbf{L}$  is symmetric positive semi-definite. Thus,

$$\lambda_{\min}(\mathbf{M}) \geq \lambda_{\min}(\mathbf{L}) = \frac{2}{3}q_{X,\Gamma} + \frac{2}{4}q_{X,\Gamma} \cos\left(\frac{N\pi}{N+1}\right) \geq \frac{q_{X,\Gamma}}{6}, \quad (30)$$

with probability higher than  $1 - \frac{1}{N}$ , where we used Theorem 2.2 in [27].

Since  $V_n$  is continuous and bounded by the assumption in Proposition 4.2, it is clear that  $AV_n$  is also bounded (see [25]). This implies that  $|V_n(x)AV_n(x)| \leq \tilde{C} < \infty$ . By Hoeffding's inequality, with probability higher than  $1 - \frac{1}{N}$ ,

$$\langle \eta_j, A\eta_i \rangle - \frac{1}{N} \sum_{k=1}^N \eta_j(\mathbf{x}_k) A\eta_i(\mathbf{x}_k) \leq \tilde{C} \left( \frac{\log N}{N} \right)^{1/2},$$

for i.i.d. samples  $X = \{\mathbf{x}_i\}_{i=1,\dots,N} \subset \Gamma$ . By Proposition 4.2, with probability higher than  $1 - \frac{24}{N}$

$$\langle \eta_j, A\eta_i \rangle \leq \frac{1}{N} \sum_{k=1}^N \eta_j(\mathbf{x}_k) A\eta_i(\mathbf{x}_k) + \tilde{C} \left( \frac{\log N}{N} \right)^{1/2} \leq \frac{1}{N} \sum_{k=1}^N \eta_j(\mathbf{x}_k) (\mathbf{A}\eta_i)_k + \underbrace{\frac{1}{N} \sum_{k=1}^N \eta_j(\mathbf{x}_k) \epsilon(N) + \tilde{C} \left( \frac{\log N}{N} \right)^{1/2}}_{=\delta(N)},$$

where we have denoted the upper bound in Proposition 4.2 as,  $A\eta_i(\mathbf{x}_k) - (\mathbf{A}\eta_i)_k \leq \epsilon(N)$ . Thus,

$$\delta(N) \leq \tilde{\delta}(N) = \frac{1}{\sqrt{N}} \|\boldsymbol{\eta}\|^2 \epsilon(N) + \tilde{C} \left( \frac{\log N}{N} \right)^{1/2} = \mathcal{O}\left(\frac{(\log N)^{\ell+2}}{N^{\ell-\frac{3}{2}}}\right) + \mathcal{O}\left(\frac{\log(N)}{N}\right)^{\min\{\frac{1}{2}, q+\frac{1}{2}\}}.$$

This implies that,

$$\begin{aligned} \langle V_N, AV_N \rangle &= \sum_{i,j=1}^N V_n(\mathbf{x}_i) V_n(\mathbf{x}_j) \langle \eta_j, A\eta_i \rangle \leq \sum_{i,j=1}^N \frac{1}{N} \sum_{k=1}^N V_n(\mathbf{x}_j) \eta_j(\mathbf{x}_k) (\mathbf{A}\eta_i)_k V_n(\mathbf{x}_i) + \sum_{i,j=1}^N V_n(\mathbf{x}_i) V_n(\mathbf{x}_j) \tilde{\delta}(N) \\ &= \frac{1}{N} \sum_{k=1}^N V_n(\mathbf{x}_k) (\mathbf{AV}_n)_k + \sum_{i,j=1}^N V_n(\mathbf{x}_i) V_n(\mathbf{x}_j) \tilde{\delta}(N) \\ &\leq \frac{1}{N} \sum_{k=1}^N V_n(\mathbf{x}_k) (\mathbf{AV}_n)_k + N \|\mathbf{V}_n\|^2 \tilde{\delta}(N), \end{aligned} \quad (31)$$

where we applied the Cauchy-Schwartz inequality. Combining (28), (30), and (31), we have

$$\frac{1}{N} \mathbf{V}_n^\top \mathbf{A} \mathbf{V}_n \geq (\zeta C q_{X,\Gamma} - N \tilde{\delta}(N)) \|\mathbf{V}_n\|^2, \quad (32)$$

which is positive definite when  $\zeta > C^{-1} N q_{X,\Gamma}^{-1} \tilde{\delta}(N)$ . By (23), with probability higher than  $1 - \frac{1}{N}$ ,  $q_{X,\Gamma} \leq h_{X,\Gamma} \leq N^{-1} \log(N)$ , then it is clear that,  $\zeta > C^{-1} (\log N)^{-1} \tilde{\delta}(N)$ . Therefore, the matrix  $\mathbf{A}$  is positive and it is, therefore, invertible. The statement of the theorem is complete by counting the probability.  $\square$

With Propositions 4.2, 4.3 and 4.5, we conclude the following convergence result for the system  $\mathbf{A}\tilde{\mathbf{V}}_n = \mathbf{b}$ . Particularly, we deduce the error of  $\tilde{\mathbf{V}}_n$  as a discrete approximation to  $\mathbf{V}_n$ , whose components are defined as  $(\mathbf{V}_n)_i = V_n(\mathbf{x}_i)$  that satisfy  $AV_n(\mathbf{x}_i) = b(\mathbf{x}_i)$  for all  $i = 1, \dots, N$ .

**Theorem 4.1.** *Let the assumptions in Propositions 4.2, 4.3, and 4.5 be valid. Then with probability higher than  $1 - \frac{58}{N}$ ,*

$$\|\mathbf{V}_n - \tilde{\mathbf{V}}_n\| = \mathcal{O}\left(\frac{(\log N)^{\ell+2}}{N^{\ell-\frac{3}{2}}}\right) + \mathcal{O}\left(\left(\frac{(\log N)^q}{N^{q+\frac{1}{2}}}\right)\right),$$

for all  $\mathbf{x}_i \in X \subset \Gamma$ , as  $N \rightarrow \infty$ .

*Proof.* Define  $\tilde{\zeta} = \zeta C h - N \tilde{\delta}(N) > 0$ . Let  $\mathbf{E} := \mathbf{V}_n - \tilde{\mathbf{V}}_n$ , then with probability higher than  $1 - \frac{25}{N}$ ,

$$\|\mathbf{E}\|^2 \leq \frac{1}{\tilde{\zeta} N} \mathbf{E}^\top \mathbf{A} \mathbf{E} \leq \frac{1}{\tilde{\zeta} N} \|\mathbf{E}\| \|\mathbf{A}\mathbf{E}\|.$$

We note that for any  $i = 1, \dots, N$ , with probability higher than  $1 - \frac{58}{N}$ ,

$$\begin{aligned} |(\mathbf{AE})_i| &= |(\mathbf{AV}_n)_i - (\mathbf{A}\tilde{\mathbf{V}}_n)_i - (AV_n)(\mathbf{x}_i) + (AV_n)(\mathbf{x}_i)| \leq |(\mathbf{AV}_n)_i - (AV_n)(\mathbf{x}_i)| + |b(\mathbf{x}_i) - \mathbf{b}_i| \\ &= \mathcal{O}\left(\frac{(\log N)^{\ell+2}}{N^{\ell-2}}\right) + \mathcal{O}\left(\left(\frac{\log N}{N}\right)^q\right), \end{aligned} \quad (33)$$

as  $N \rightarrow \infty$ . So,

$$\|\mathbf{E}\| \leq \frac{1}{\tilde{\zeta}N} \|\mathbf{AE}\| = \frac{1}{\tilde{\zeta}N^{1/2}} \left( \mathcal{O}\left(\frac{(\log N)^{\ell+2}}{N^{\ell-2}}\right) + \mathcal{O}\left(\left(\frac{\log N}{N}\right)^q\right) \right),$$

which vanishes as  $N \rightarrow \infty$ .  $\square$

## 5 Numerical Experiments

In this section, we present numerical experiments for (2) on a variety of smooth closed curves to illustrate the effectiveness of the proposed algorithms. Convergence studies are carried out for the circular case, where the exact solution is available. For simplicity, we use  $k = \sqrt{N}$  (number of KNN to be used, chosen to be an odd number) where  $N$  is the number of sampling points and degree  $\ell = 6$  polynomial with uniformly sampled initial data points in the GMLS approximation for all examples.

### 5.1 Free boundary equation on circle

First, we consider the free boundary equation with a prescribed time-dependent forcing term,  $h(t)$ ,

$$\begin{cases} -\Delta p = 0 & \text{in } \Omega(t), \\ p = \kappa & \text{on } \Gamma(t), \\ \frac{\partial p}{\partial \mathbf{n}} = -V_n + h(t) & \text{on } \Gamma(t), \end{cases} \quad (34)$$

where  $h(t) = 500 \cos(500\pi t)$ .

Then, integrating the equations on the free boundary leads to the following system,

$$\begin{cases} \int_{\Gamma} G(\mathbf{x}, \mathbf{y}) (V_n(\mathbf{y}) - h(t)) dS_{\mathbf{y}} = -\frac{\kappa(\mathbf{x})}{2} - \int_{\Gamma} \kappa(\mathbf{y}) \frac{\partial G(\mathbf{x}, \mathbf{y})}{\partial \mathbf{n}(\mathbf{y})} dS_{\mathbf{y}}, & \mathbf{x}, \mathbf{y} \in \Gamma(t), \\ \frac{d\mathbf{x}}{dt} = V_n(\mathbf{x}) \mathbf{n}(\mathbf{x}), & \mathbf{x} \in \Gamma(t), \end{cases} \quad (35)$$

With the initial condition given by the unit circle,

$$\mathbf{x}(0) = (x_1(0), x_2(0)) = (\cos(\theta), \sin(\theta)), \quad \theta \in [0, 2\pi], \quad (36)$$

The solution at any time  $t$  is given by

$$\begin{aligned} R(t) &= 1 + \frac{1}{\pi} \sin(500\pi t), \\ \mathbf{x}(t) &= (x_1(t), x_2(t)) = (R(t) \cos(\theta), R(t) \sin(\theta)), \quad \theta \in [0, 2\pi], \end{aligned}$$

where  $R(t)$  represents the radius of circle. Then we conduct the mesh refinement tests to check the order of spatial convergence and temporal convergence. First, we apply our method to discretize (35) directly on point clouds with  $N = 100, 200, 400, 800$ , and use forward Euler (3.1) with time step  $\Delta t = 10^{-5}$ . We quantify the numerical error in approximating  $V_n(\mathbf{x})$  with,

$$\|e_V\|_{L^2} = \sqrt{\frac{1}{|\Gamma|} \int_{\Gamma} \|\tilde{\mathbf{V}}_n(\mathbf{x}) - V_n(\mathbf{x})\|^2 dS_{\mathbf{x}}} \approx \sqrt{\frac{1}{N} \sum_{i=1}^N ((\tilde{\mathbf{V}}_n)_i - V_n(\mathbf{x}_i))^2},$$

at the time  $t = 10^{-3}$ . In Figure 2(a), we show the convergence results corresponding to two numerical quadrature rules, the trapezoidal and Simpson's rule, applied in approximation of  $b$  (see (20)). As for the approximation of  $A$ , we consider the trapezoidal rule (with the discrete component  $\mathbf{A}_{ij}$  as reported above (20)). For this particular example, notice that the error rate of Simpson is better than that of the trapezoidal despite the fact that the operator

$A$  is discretized with the same trapezoidal rule. The main reason here is that in this circular case, the first term in Eqn. (35) can be written as  $AV_n(\mathbf{x}) = b(\mathbf{x}) + h(t)\mathbf{A}\mathbf{1}(\mathbf{x})$ , where  $b(\mathbf{x}) = 0$  for the circle and  $V_n(\mathbf{x}) = h(t)\mathbf{1}(\mathbf{x})$ . Denoting the approximation of  $\mathbf{A} = A + \delta A$  and  $\mathbf{b} = b(\mathbf{x}) + \delta b = \delta b$ , and  $\mathbf{V}_n = V_n(\mathbf{x}) + \delta V_n$ , where the “delta” terms denote the corresponding numerical errors, one can deduce that  $(A + \delta A)\delta V_n = \delta b$ . Applying the Woodbury identity, we obtain  $\delta V_n = (I + A^{-1}\delta A)^{-1}A^{-1}\delta b$ , which explains why the error rate is dominated by the error induced by the quadrature rule in the estimation of  $b$  as observed in Figure 2(a).

Next, we conduct the time convergence studies with  $N = 400$  and calculate the numerical solutions to  $t = 4 \times 10^{-3}$  with various time steps. The max-norm relative errors  $\|e_R\|_{\ell^\infty}$  for radius of the circle using forward Euler (3.1) and second-order Runge Kutta (3.2) are reported in Figure 2(b). It indicates the first-order accuracy in time with the forward Euler method and second-order accuracy in time with the second-order Runge-Kutta method. Also, the evolution dynamics with  $N = 400$ ,  $\Delta t = 10^{-5}$ , and forward Euler method are shown in Figure 3(a) which depicts the boundary at various times,  $t = 0, 0.001$ , and  $0.003$ . The absolute error in the radius over time is shown in Figure 3(b), where the errors exhibit oscillations with a period of approximately  $4 \times 10^{-3}$ .

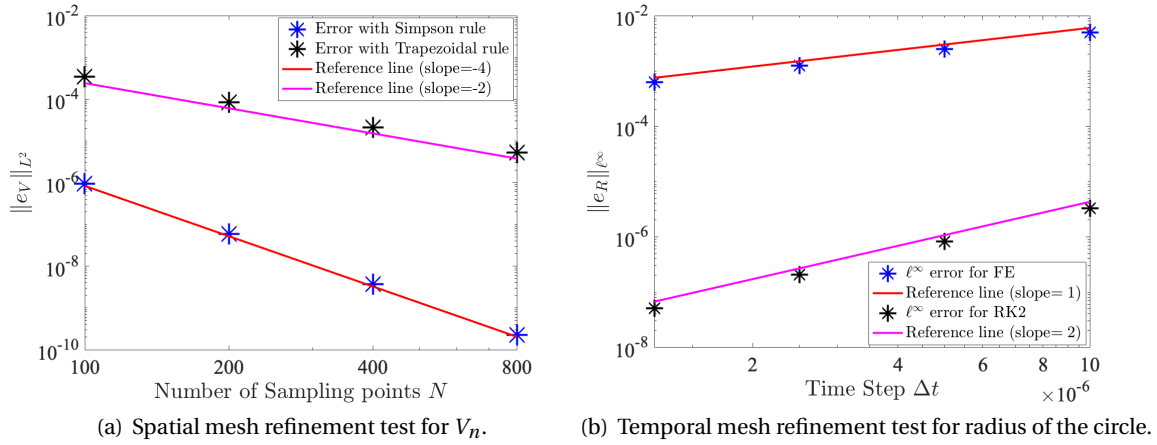
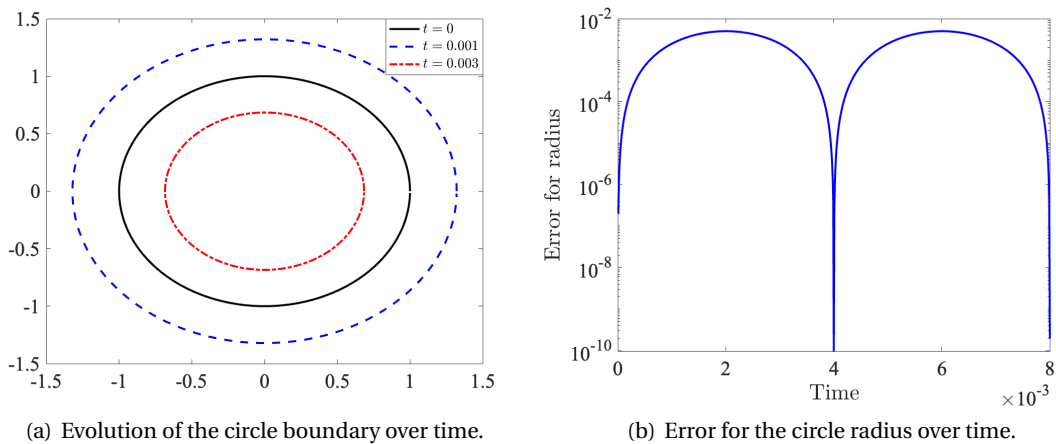


Figure 2: Mesh refinement tests.

Figure 3: The evolution dynamics for the circular case. In (a), the profiles of  $\mathbf{x}(t)$  at  $t = 0, 0.001, 0.003$  are shown; (b) The errors for radius  $R(t)$  are plotted at a time interval  $[0, 8 \times 10^{-3}]$ .

## 5.2 Free boundary equation on perturbations of a circle

In this section, we consider the free boundary equation (2) with the initial condition given by perturbations of a circle,

$$\begin{aligned} r(\theta) &= r_0 + D_1 \cos(D_2 \theta), \\ \mathbf{x}(0) &= (x_1(0), x_2(0)) = (r(\theta) \cos(\theta), r(\theta) \sin(\theta)), \quad \theta \in [0, 2\pi], \end{aligned} \quad (37)$$

where  $D_1$  and  $D_2$  are parameters. First, we can observe that the area of  $\Omega(t)$  is conserved for (1) with  $f = 0$ ,

$$\frac{d}{dt} |\Omega(t)| = \int_{\Gamma} V_n(\mathbf{x}) dS_{\mathbf{x}} = - \int_{\Gamma} \frac{\partial p(\mathbf{x})}{\partial \mathbf{n}(\mathbf{x})} dS_{\mathbf{x}} = - \int_{\Omega} \Delta p d\Omega = 0.$$

Thus the area of the steady-state circle with the initial condition given in (37) is

$$\text{Area} = \frac{1}{2} \int_0^{2\pi} (r_0 + D_1 \cos(D_2 \theta))^2 d\theta = \pi r_0^2 + \frac{\pi}{2} D_1^2,$$

which implies the radius of the steady-state circle is

$$r_s = \sqrt{r_0^2 + \frac{D_1^2}{2}}.$$

We then examine the evolution dynamics for different  $D_1, D_2$ , using the trapezoidal rule to approximate  $A$ , Simpson's rule to approximate  $b$ , and the forward Euler method with  $\Delta t = 10^{-5}$  and  $N = 400$ , and  $r_0 = 1$ . Then we compare the radius of numerical solutions with  $r_s$ . We point out that when  $N = 400$ ,  $D_1 = 0.3$ , and  $D_2 = 5$ , we redistribute mesh points onto an equispaced mesh using cubic spline interpolation to prevent point collapse during boundary evolution. The results are summarized in Figure 4. Figure 4 (a), (c), and (e) present the boundary evolution dynamics for different perturbations of the circle under varying  $D_1$  and  $D_2$  in (37), with initial conditions shown as black curves. The results indicate that the boundaries approach a circle of radius  $r_s$ , as predicted by the conservation of area. Furthermore, we examine the maximum and minimum distances from the boundary points to the center, defined as  $d_i = \|\mathbf{x}_i - \mathbf{x}_*\|$ ,  $i = 1, \dots, N$  with  $\mathbf{x}_* = \frac{\int_{\Gamma} \mathbf{x} dS_{\mathbf{x}}}{\int_{\Gamma} dS_{\mathbf{x}}}$  being the center of  $\Omega(t)$ , and compare them with  $r_s$  in Figure 4 (b), (d), and (e). This quantitatively demonstrates that the radii of the estimated curves converge to  $r_s$ .

## 5.3 Free boundary equation on smooth closed curves

In this section, we apply our method to smooth closed curves, including a heart-shaped curve and a roughly humanoid-shaped curve. Specifically, we use the trapezoidal rule to approximate  $A$ , Simpson's rule to approximate  $b$ , and the forward Euler method with  $\Delta t = 10^{-5}$ ,  $N = 400$ , and redistribute mesh points onto an equispaced mesh using cubic spline interpolation to prevent point collapse during boundary evolution.

First, we consider the heart-shaped curve, whose initial condition is given as

$$\mathbf{x}(0) = (x_1(0), x_2(0)) = (\sin(\theta), 1.5 \cos(\theta) - 0.4 \cos(2\theta) - 0.1 \cos(3\theta) - 0.1 \cos(4\theta)), \quad \theta \in [0, 2\pi].$$

Furthermore, we study the evolution dynamics of a roughly humanoid-shaped curve. The curve is initially defined by 25 points, which are interpolated to generate 400 points that serve as its initial configuration. The results are summarized in Figure 5. Figure 5 (a) and (c) present the boundary evolution dynamics for different initial conditions shown as black curves. The results indicate that the boundaries approach a circle, which is quantitatively demonstrated in Figure 5 (b) and (d) by comparing the maximum and minimum distances from the boundary points to the center.

## 6 Conclusion

In this paper, we have introduced a novel meshfree computational framework for solving the two-dimensional Hele-Shaw problem with surface tension. The core of our approach is a geometric local parameterization of the moving boundary via GMLS, enabling accurate and robust treatment of complex, evolving geometries represented solely by point clouds.

Our main contributions are as follows 1) **GMLS-based Discretization:** We developed a numerical scheme that systematically discretizes the singular boundary integral formulation of the Hele-Shaw problem. By constructing

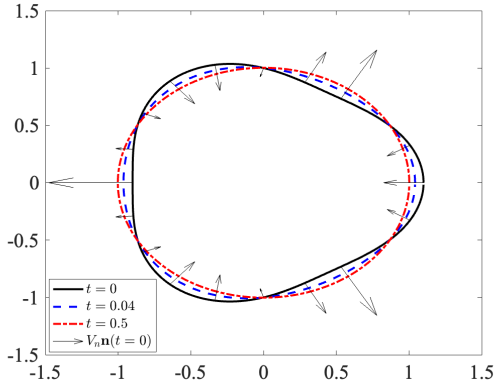
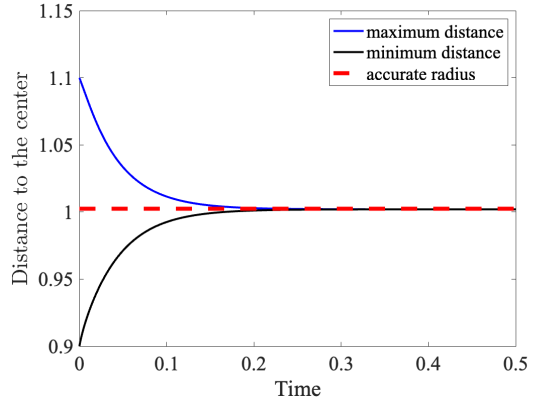
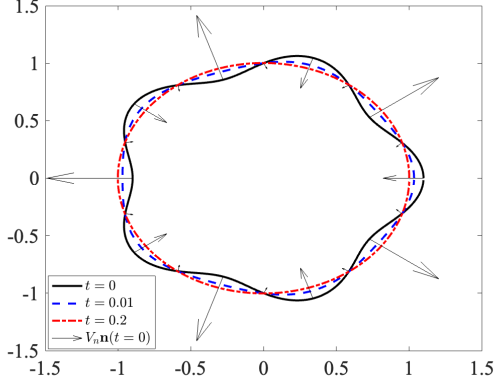
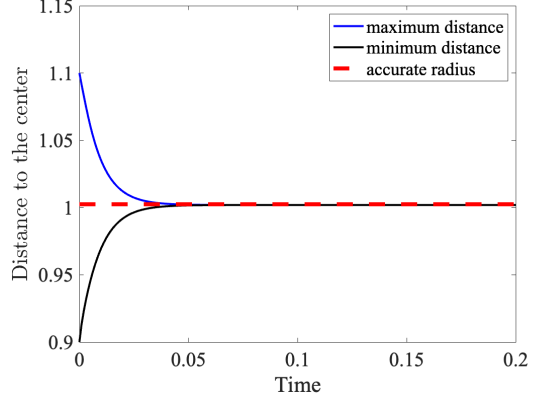
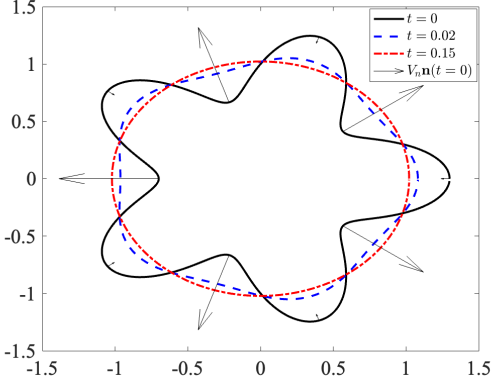
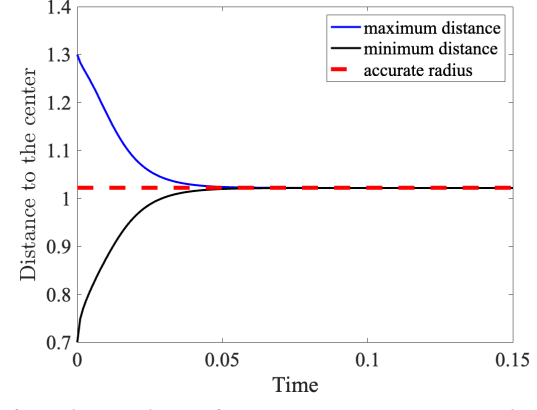
(a) Evolution dynamics for  $D_1 = 0.1, D_2 = 3$ .(b) Radius evolution for  $D_1 = 0.1, D_2 = 3$  compared with steady-state value.(c) Evolution dynamics for  $D_1 = 0.1, D_2 = 5$ .(d) Radius evolution for  $D_1 = 0.1, D_2 = 5$  compared with steady-state value.(e) Evolution dynamics for  $D_1 = 0.3, D_2 = 5$ .(f) Radius evolution for  $D_1 = 0.3, D_2 = 5$  compared with steady-state value.

Figure 4: The evolution dynamics for perturbed circles with different  $D_1$  and  $D_2$ . In (a), (c), and (e), the profiles of  $\mathbf{x}(t)$  at different times and boundary motion  $V_n \mathbf{n}$  at  $t = 0$  for different  $D_1$  and  $D_2$  are shown. In (b), (d), and (f), comparisons of the maximum and minimum distances from the boundary points to the center with the steady-state circle radius  $r_s$  for different  $D_1$  and  $D_2$  are shown, where we observe that the perturbed circles with different  $D_1$  and  $D_2$  evolve into circles with radius  $r_s$ .

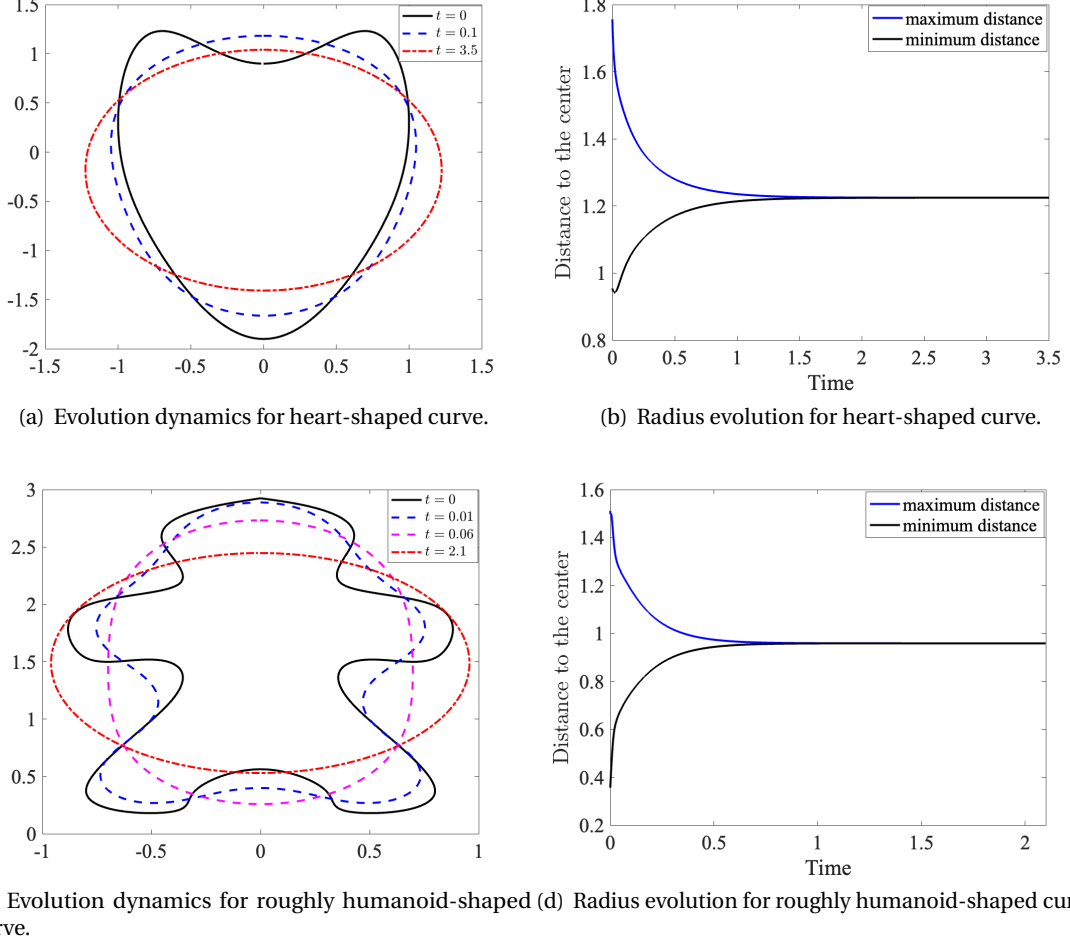


Figure 5: The evolution dynamics for smooth closed curves. In (a) and (c), the profiles of  $\mathbf{x}(t)$  at different times are shown. In (b) and (d), the maximum and minimum distances from the boundary points to the center are shown, where we observe that the smooth closed curves evolve into circles.

local charts via GMLS, we accurately approximate geometric quantities such as normal vectors and curvature, and handle the singular integrals arising from the Green's function by analytically isolating the logarithmic singularity and applying local quadratic interpolation to the rest to maintain second-order accuracy. 2) **Theoretical Analysis:** We provided a rigorous theoretical foundation for the proposed method. This includes a detailed error analysis demonstrating the spatial consistency of our discretization for the boundary integral operators and establishing the invertibility of the resulting linear system under appropriate conditions. Our analysis reveals that the convergence rate is determined by the smoothness of the underlying boundary and the order of the quadrature rules that are used in approximating the boundary integral equation. 3) **Numerical Verification:** We validated the effectiveness and accuracy of our method through a series of numerical experiments. Convergence studies on a circle confirmed the high-order spatial accuracy and the expected temporal convergence of the time discretization schemes. Furthermore, simulations on perturbed circles and more complex smooth curves (e.g., heart-shaped and humanoid-shaped boundaries) demonstrated the method's robustness and its ability to capture the correct long-time dynamics, where the evolving boundaries, besides circles, as predicted by area conservation and surface tension effects.

The proposed method offers a powerful and flexible alternative to traditional parameterized boundary integral methods, particularly for problems where maintaining a global parameterization is difficult or where complex topological changes may occur in future extensions. Several directions for future research follow from this work. A natural extension is to handle problems with a source term, namely,  $f(\mathbf{x}) \neq 0$ , which arise in biological applications like tumor growth. Developing adaptive mesh refinement strategies would also enhance efficiency for long-time simulations or boundaries with high-curvature regions. Finally, the most significant challenge and opportunity

is the generalization to three-dimensional Hele-Shaw problems and other free-boundary problems, where the advantages of avoiding global parameterization would be particularly impactful.

## Acknowledgment

The research of JH was partially supported under the NSF grants DMS-2209535 and DMS-2505605, and the ONR grant N00014-22-1-2193. WH was supported by the National Institute of General Medical Sciences through grant 1R35GM146894. ZZ was partially supported under the ICDS seed grant.

## A Proof of Proposition 4.3

For simplicity, we define

$$b(\mathbf{x}_i) = -\frac{\kappa(\mathbf{x}_i)}{2} + \frac{1}{2} I_b^*,$$

where

$$I_b^* = -\sum_j \int_{\Delta s(\mathbf{x}_{-j})}^{\Delta s(\mathbf{x}_j)} \kappa(\iota(s)) (\nabla G(\mathbf{x}_i, \iota(s)) \cdot \mathbf{n}(\iota(s))) \sqrt{|\iota'(s)|} ds.$$

By Proposition 3.1 and Proposition 4.1, with probability higher than  $1 - \frac{1}{N}$ ,

$$|\kappa(\mathbf{x}_i) - \kappa_i| = \mathcal{O}\left(\left(\frac{\log N}{N}\right)^{\ell-1}\right). \quad (38)$$

Then we consider the error bound for  $|I_b^* - \tilde{I}_b|$ . Note that

$$\begin{aligned} |I_b^* - \tilde{I}_b| &\leq |I_b^* - I_b| + |I_b - \tilde{I}_b| \\ &= \sum_j \left| \int_{\Delta s(\mathbf{x}_{-j})}^{\Delta s(\mathbf{x}_j)} (\nabla G(\mathbf{x}_i, \iota(s)) \cdot \mathbf{n}(\iota(s))) \phi^*(s) ds - \int_{\Delta s_{-j}}^{\Delta s_j} (\nabla G(\mathbf{x}_i, \iota_j(s)) \cdot \hat{\mathbf{n}}(\iota_j(s))) \phi_j(s) ds \right| + \mathcal{O}\left(\left(\frac{\log N}{N}\right)^q\right), \end{aligned}$$

where  $\tilde{I}_b$  is the quadrature rule approximation to  $I_b$  with error of order- $q$ , and  $\phi^*(s) := \kappa(\iota(s)) \sqrt{|\iota'(s)|}$ ,  $\phi_j(s) := \kappa(\iota_j(s)) \sqrt{1 + (p'_j(s))^2}$ .

By Proposition 3.1, with probability higher than  $1 - \frac{2}{N}$ .

$$\begin{aligned} |\phi^*(s) - \phi_j(s)| &= \left| \kappa(\iota(s)) \sqrt{|\iota'(s)|} - \kappa(\iota_j(s)) \sqrt{1 + (p'_j(s))^2} \right| \\ &\leq |\kappa(\iota(s))| \left| \sqrt{|\iota'(s)|} - \sqrt{1 + (p'_i(s))^2} \right| + \sqrt{1 + (p'_i(s))^2} |\kappa(\iota(s)) - \kappa_i(s)| \\ &= \mathcal{O}\left(\left(\frac{\log N}{N}\right)^\ell\right) + \mathcal{O}\left(\left(\frac{\log N}{N}\right)^{\ell-1}\right) = \mathcal{O}\left(\left(\frac{\log N}{N}\right)^{\ell-1}\right). \end{aligned}$$

Then, with probability higher than  $1 - \frac{4}{N}$ ,

$$\begin{aligned} &|\nabla G(\mathbf{x}_i, \iota(s)) \cdot \mathbf{n}(\iota(s)) \phi^*(s) - \nabla G(\mathbf{x}_i, \iota_j(s)) \cdot \hat{\mathbf{n}}(\iota_j(s)) \phi_j(s)| \\ &\leq |\nabla G(\mathbf{x}_i, \iota(s)) \cdot \mathbf{n}(\iota(s)) - \nabla G(\mathbf{x}_i, \iota_j(s)) \cdot \hat{\mathbf{n}}(\iota_j(s))| |\phi^*(s)| + |\nabla G(\mathbf{x}_i, \iota_j(s)) \cdot \hat{\mathbf{n}}(\iota_j(s))| |\phi^*(s) - \phi_j(s)| \\ &\leq |\nabla G(\mathbf{x}_i, \iota(s)) \cdot (\mathbf{n}(\iota(s)) - \hat{\mathbf{n}}(\iota_j(s)))| |\phi^*(s)| + |(\nabla G(\mathbf{x}_i, \iota(s)) - \nabla G(\mathbf{x}_i, \iota_j(s))) \cdot \hat{\mathbf{n}}(\iota_j(s))| |\phi^*(s)| + \mathcal{O}\left(\left(\frac{\log N}{N}\right)^{\ell-1}\right) \\ &= C \frac{|\mathbf{x}_i - \iota(s)| \cdot |\mathbf{n}(\iota(s)) - \hat{\mathbf{n}}(\iota_j(s))|}{\|\mathbf{x}_i - \iota(s)\|^2} + C \left| \frac{-\|\mathbf{x}_i - \iota(s)\|^2 \mathbf{1}_2 + 2(\mathbf{x}_i - \iota(s)) \odot (\mathbf{x}_i - \iota(s))}{\|\mathbf{x}_i - \iota(s)\|^4} \odot (\iota(s) - \iota_j(s)) \cdot \hat{\mathbf{n}}(\iota_j(s)) \right| \\ &\quad + \mathcal{O}\left(\left(\frac{\log N}{N}\right)^{\ell-1}\right) \\ &= \mathcal{O}\left(\frac{(\log N)^\ell}{N^{\ell-2}}\right) + \mathcal{O}\left(\frac{(\log N)^{\ell+1}}{N^{\ell-3}}\right) + \mathcal{O}\left(\left(\frac{\log N}{N}\right)^{\ell-1}\right) = \mathcal{O}\left(\frac{(\log N)^{\ell+1}}{N^{\ell-3}}\right) \end{aligned}$$

where  $\mathbf{1}_2 = [1, 1]^\top$  and  $\odot$  represents the Hadamard product.

Therefore, with probability higher than  $1 - \frac{9}{N}$ ,

$$\begin{aligned}
|I_b^* - I_b| &\leq \sum_j \left| \int_{\Delta s(\mathbf{x}_{-j})}^{\Delta s(\mathbf{x}_j)} (\nabla G(\mathbf{x}_i, \iota(s)) \cdot \mathbf{n}(\iota(s))) \phi^*(s) ds - \int_{\Delta s_{-j}}^{\Delta s_j} (\nabla G(\mathbf{x}_i, \iota(s)) \cdot \mathbf{n}(\iota(s))) \phi^*(s) ds \right| \\
&\quad + \sum_j \left| \int_{\Delta s_{-j}}^{\Delta s_j} (\nabla G(\mathbf{x}_i, \iota(s)) \cdot \mathbf{n}(\iota(s))) \phi^*(s) ds - \int_{\Delta s_{-j}}^{\Delta s_j} (\nabla G(\mathbf{x}_i, \iota_j(s)) \cdot \hat{\mathbf{n}}(\iota_j(s))) \phi_j(s) ds \right| \\
&= C(|\Delta s_i - \Delta s(\mathbf{x}_i)| + |\Delta s_{-i} - \Delta s(\mathbf{x}_{-i})|) \\
&\quad + \max_{s \in [\Delta s_{-i}, \Delta s_i]} |\nabla G(\mathbf{x}_i, \iota(s)) \cdot \mathbf{n}(\iota(s)) \phi^*(s) - \nabla G(\mathbf{x}_i, \iota_j(s)) \cdot \hat{\mathbf{n}}(\iota_j(s)) \phi_j(s)| |\Delta s_i - \Delta s_{-i}| \\
&= \mathcal{O}\left(\left(\frac{\log N}{N}\right)^{\ell+1}\right) + \mathcal{O}\left(\frac{(\log N)^{\ell+2}}{N^{\ell-2}}\right) = \mathcal{O}\left(\frac{(\log N)^{\ell+2}}{N^{\ell-2}}\right).
\end{aligned}$$

Finally, we have

$$|I_b^* - \tilde{I}_b| \leq |I_b^* - I_b| + |I_b - \tilde{I}_b| = \mathcal{O}\left(\frac{(\log N)^{\ell+2}}{N^{\ell-2}}\right) + \mathcal{O}\left(\left(\frac{\log N}{N}\right)^q\right). \quad (39)$$

With the bounds in (38) and (39), the proof is completed.

## References

- [1] Vasilios Alexiades. *Mathematical modeling of melting and freezing processes*. Routledge, 2018.
- [2] X. Chen and A. Friedman. A free boundary problem for an elliptic-hyperbolic system: an application to tumor growth. *SIAM Journal on Mathematical Analysis*, 35(4):974–986, 2003.
- [3] Ronald R Coifman and Stéphane Lafon. Diffusion maps. *Applied and computational harmonic analysis*, 21(1):5–30, 2006.
- [4] P. Constantin and M Pugh. Global solutions for small data to the hele-shaw problem. *Nonlinearity*, 6(3):393, 1993.
- [5] Vittorio Cristini, John Lowengrub, and Qing Nie. Nonlinear simulation of tumor growth. *Journal of mathematical biology*, 46(3):191–224, 2003.
- [6] E. DiBenedetto and A. Friedman. The ill-posed hele-shaw model and the stefan problem for supercooled water. *Transactions of the American Mathematical Society*, 282(1):183–204, 1984.
- [7] A. Friedman. Free boundary problems in biology. *Phil. Trans. R. Soc. A*, 373(2050):20140368, 2015.
- [8] A. Friedman and W. Hao. A mathematical model of atherosclerosis with reverse cholesterol transport and associated risk factors. *Bulletin of mathematical biology*, 77(5):758–781, 2015.
- [9] A. Friedman and J. Spruck. *Variational and free boundary problems*, volume 53. Springer Science & Business Media, 2012.
- [10] Avner Friedman. *Generalized functions and partial differential equations*. Prentice Hall, 1963.
- [11] Ben J Gross, Nathaniel Trask, Paul Kuberry, and Paul J Atzberger. Meshfree methods on manifolds for hydrodynamic flows on curved surfaces: A Generalized Moving Least-Squares (GMLS) approach. *J. Comput. Phys.*, 409:109340, 2020.
- [12] Sushil Chandra Gupta. *The classical Stefan problem: basic concepts, modelling and analysis with quasi-analytical solutions and methods*, volume 45. Elsevier, 2017.
- [13] W. Hao, E. Crouser, and A. Friedman. Mathematical model of sarcoidosis. *Proceedings of the National Academy of Sciences*, 111(45):16065–16070, 2014.
- [14] W. Hao and A. Friedman. The LDL-HDL profile determines the risk of atherosclerosis: a mathematical model. *PLoS ONE*, 9(3):e90497, 2014.
- [15] W. Hao, J. Hauenstein, B. Hu, Y. Liu, A. Sommese, and Y.-T. Zhang. Bifurcation for a free boundary problem modeling the growth of a tumor with a necrotic core. *Nonlinear Analysis: Real World Applications*, 13(2):694–709, 2012.

- [16] W. Hao, J. Hauenstein, B. Hu, T. McCoy, and A. Sommese. Computing steady-state solutions for a free boundary problem modeling tumor growth by stokes equation. *Journal of Computational and Applied Mathematics*, 237(1):326–334, 2013.
- [17] W. Hao, J. Hauenstein, B. Hu, and A. Sommese. A three-dimensional steady-state tumor system. *Applied Mathematics and Computation*, 218(6):2661–2669, 2011.
- [18] W. Hao, B. Hu, and A. Sommese. Numerical algebraic geometry and differential equations. In *Future Vision and Trends on Shapes, Geometry and Algebra*, pages 39–53. Springer, 2014.
- [19] Wenrui Hao. A homotopy method for parameter estimation of nonlinear differential equations with multiple optima. *Journal of Scientific Computing*, 74(3):1314–1324, 2018.
- [20] John Harlim, Shixiao Willing Jiang, and John Wilson Peoples. Radial basis approximation of tensor fields on manifolds: from operator estimation to manifold learning. *Journal of Machine Learning Research*, 24(345):1–85, 2023.
- [21] H. Hele-Shaw. Flow of water. *Nature*, 58:520, 1898.
- [22] Thomas Y Hou, Zhilin Li, Stanley Osher, and Hongkai Zhao. A hybrid method for moving interface problems with application to the hele–shaw flow. *Journal of Computational Physics*, 134(2):236–252, 1997.
- [23] Shixiao Willing Jiang and John Harlim. Ghost point diffusion maps for solving elliptic PDEs on manifolds with classical boundary conditions. *Communications on Pure and Applied Mathematics*, 76(2):337–405, 2023.
- [24] Shixiao Willing Jiang, Rongji Li, Qile Yan, and John Harlim. Generalized finite difference method on unknown manifolds. *Journal of Computational Physics*, 502:112812, 2024.
- [25] Rainer Kress. *Linear integral equations*, volume 82. Springer, 1989.
- [26] Rainer Kress. *Linear integral equations*, volume 82. Springer, 1999.
- [27] Devadatta Kulkarni, Darrell Schmidt, and Sze-Kai Tsui. Eigenvalues of tridiagonal pseudo-toeplitz matrices. *Linear Algebra and its Applications*, 297:63–80, 1999.
- [28] Shuwang Li, John S Lowengrub, and Perry H Leo. A rescaling scheme with application to the long-time simulation of viscous fingering in a hele–shaw cell. *Journal of Computational Physics*, 225(1):554–567, 2007.
- [29] Jian Liang and Hongkai Zhao. Solving partial differential equations on point clouds. *SIAM J. Sci. Comput.*, 35(3):A1461–A1486, 2013.
- [30] Min-Jhe Lu, Wenrui Hao, Bei Hu, and Shuwang Li. Bifurcation analysis of a free boundary model of vascular tumor growth with a necrotic core and chemotaxis. *Journal of mathematical biology*, 86(1):19, 2023.
- [31] Paul Macklin and John Lowengrub. An improved geometry-aware curvature discretization for level set methods: application to tumor growth. *Journal of Computational Physics*, 215(2):392–401, 2006.
- [32] W McLean. Variation properties of some simple boundary integral equations. In *Theoretical and Numerical Aspects of Geometric Variational Problems*, volume 26, pages 168–179. Australian National University, Mathematical Sciences Institute, 1991.
- [33] Davoud Mirzaei, Robert Schaback, and Mehdi Dehghan. On generalized moving least squares and diffuse derivatives. *IMA Journal of Numerical Analysis*, 32(3):983–1000, 2012.
- [34] Alireza Mohammad Karim. A review of physics of moving contact line dynamics models and its applications in interfacial science. *Journal of Applied Physics*, 132(8), 2022.
- [35] P. Saffman and G. Taylor. The penetration of a fluid into a porous medium or hele–shaw cell containing a more viscous liquid. In *Proceedings of the Royal Society of London A: Mathematical, Physical and Engineering Sciences*, volume 245, pages 312–329. The Royal Society, 1958.
- [36] Steven Vogel. *Life in moving fluids: the physical biology of flow*. Princeton university press, 1996.
- [37] Qile Yan, Shixiao Willing Jiang, and John Harlim. Spectral methods for solving elliptic pdes on unknown manifolds. *Journal of Computational Physics*, 486:112132, 2023.